Mitochondria-containing extracellular vesicles from mouse *vs*. human brain endothelial cells for ischemic stroke therapy

Kandarp M. Dave[1], Venugopal R. Venna[2], Krithika S. Rao[3], Donna B. Stolz[4], Victoria A. Quaicoe[2], Michael E. Maniskas[2], Ella E. Hildebrand[1,5], Dawson Green[1], Mingxi Chen[6], Jadranka Milosevic[6,7], Si-yang Zheng[6], Sruti S. Shiva[3,8], Louise D. McCullough[2], Devika S Manickam[1*]

[1]Graduate School of Pharmaceutical Sciences, Duquesne University, Pittsburgh, PA

[2]Department of Neurology, McGovern Medical School, University of Texas Health Science Center, Houston, TX

[3]Pittsburgh Heart Lung Blood Vascular Institute, University of Pittsburgh Medical School, Pittsburgh, PA

[4]Center for Biologic Imaging, University of Pittsburgh Medical School, Pittsburgh, PA

[5]Department of Psychology, Westminster College, New Wilmington, PA

[6]Department of Biomedical Engineering, Carnegie Mellon University, Pittsburgh, PA,

[7]Captis Diagnostics Inc, Pittsburgh, PA

[8]Department of Pharmacology & Chemical Biology, University of Pittsburgh Medical School, Pittsburgh, PA

***Corresponding author:** Devika S Manickam
600 Forbes Avenue, 453 Mellon Hall,
Pittsburgh, PA 15282.
Email: soundaramanickd@duq.edu
Twitter: @manickam_lab
Phone: +1 (412) 396-4722

Abstract

Ischemic stroke-induced mitochondrial dysfunction in the blood-brain barrier-forming brain endothelial cells (**BECs**) results in long-term neurological dysfunction post-stroke. We previously reported that *intravenous* administration of human BEC (**hBEC**)-derived mitochondria-containing extracellular vesicles (**EVs**) showed a potential efficacy signal in a mouse middle cerebral artery occlusion (**MCAo**) model of stroke. We *hypothesized* that EVs harvested from donor species homologous to the recipient species (*e.g.*, mouse) may improve therapeutic efficacy, and therefore, use of mouse BEC (**mBEC**)-derived EVs may improve post-stroke outcomes in MCAo mice.

We investigated if EVs derived from the same species as the recipient cell (mBEC-EVs and recipient mBECs or hBECs-EVs and recipient hBECs) show a greater EV mitochondria delivery efficiency than cross-species EVs and recipient cells (mBEC-EVs and recipient hBECs or *vice versa*). Our results showed that mBEC-EVs outperformed hBEC-EVs in transferring EV mitochondria to the recipient ischemic mBECs, and improved mBEC mitochondrial function via increasing oxygen consumption rate. mBEC-EVs significantly reduced brain infarct volume and improved behavioral recovery compared to vehicle-injected MCAo mice. Our data suggests that mBEC-EVs show superior therapeutic efficacy in a mouse MCAo stroke model compared to hBEC-EVs—supporting the continued use of mBEC-EVs to optimize the therapeutic potential of mitochondria-containing EVs in preclinical studies.

Keywords Mitochondria, microvesicles, exosomes, ischemic stroke, brain endothelial cells, BBB protection

Graphical Abstract

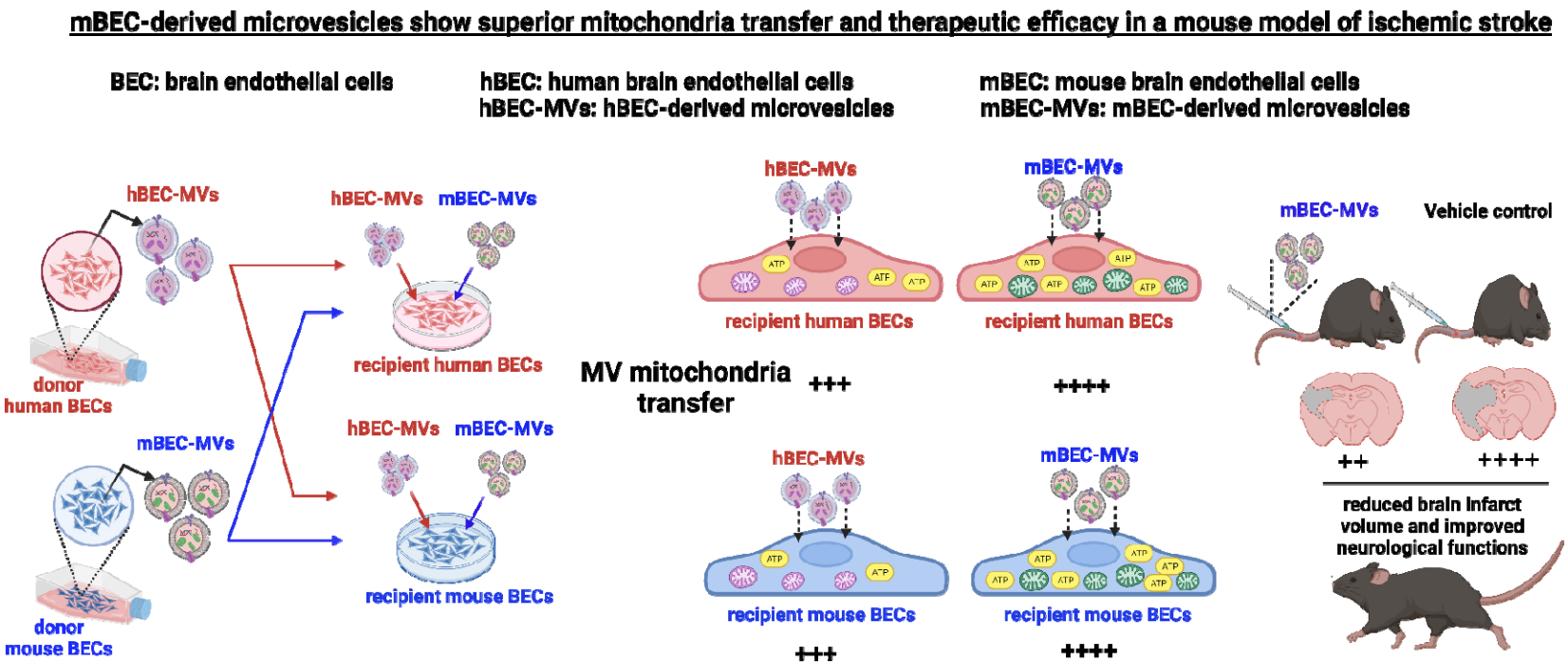

1. Introduction

Mitochondria are essential organelles that maintain cellular bioenergetics by producing adenosine triphosphate (**ATP**) and are involved in key metabolic pathways, enabling cell survival and proliferation [1-3]. Given their central role, mitochondrial damage or dysfunction produces excessive cytochrome c, reactive oxygen and nitrogen species, leading to programmed cell death. Mitochondrial dysfunction is one of the hallmarks of numerous pathological conditions [4], including ischemic stroke—the second leading cause of death worldwide [5, 6].

Ischemic stroke occurs when an obstruction in brain blood vessels reduces oxygen and nutrient supply to the affected brain regions, leading to brain damage, chronic disability, or even death [6, 7]. The blood-brain barrier (**BBB**)-forming brain endothelial cells (**BECs**) play a causal role in the pathophysiology of ischemic stroke. BECs contain about five-fold greater amounts of mitochondria than peripheral endothelial cells [8, 9]. The greater mitochondrial load in BECs is required to maintain cellular homeostasis and BBB integrity [3, 8, 10]. Oxygen-glucose deprivation (**OGD**) in BECs leads to excessive intracellular cation accumulation and glutamate excitotoxicity, impairing mitochondrial membrane potential. As a result, OGD-exposed BECs show reduced mitochondrial oxidative phosphorylation and ATP levels [10, 11], subsequently triggering cell death [12]. Therefore, maintaining BEC mitochondrial functionality is critical for cell survival. Physiologically, the damaged mitochondria are either rescued by fusion with intracellular healthy mitochondria or degraded by mitophagy—phagocytosis of damaged mitochondria by lysosomes [13]. When cells cannot recover damaged mitochondria under stress conditions, exogenous delivery of healthy mitochondria to the damaged cell could be a promising approach to mitigate mitochondrial dysfunction in ischemic stroke. No clinically

approved therapeutics deliver functional mitochondria for the treatment of mitochondrial disorders.

Numerous studies have shown that cell-derived extracellular vesicles (**EVs**) contain innate mitochondrial components such as mitochondrial DNA, proteins, and mitochondria [14-18] along with their intrinsic nucleic acids, non-mitochondrial proteins and lipid components [19]. Moreover, the natural ability of EVs to protect their innate cargo from systemic degradation [18], cross the BBB [20], and deliver their innate cargo to the target cells [21] makes them a promising carrier for drug delivery to the brain [22, 23]. Exosomes (**EXOs**) and microvesicles (**MVs**) are subtypes of EVs that differ in their biogenesis, vesicle size, and innate components [17, 24, 25]. EXOs are derived from the inward budding of endosomal membranes with characteristic particle diameters of <200 nm. MV biogenesis involves outward blebbing and pinching of plasma membranes, releasing MVs into extracellular spaces with particle diameters >200 nm [26]. Published reports have shown that EXOs selectively contain mitochondrial proteins [14] and mitochondrial DNA [15], while MVs contain mitochondrial proteins and functional mitochondria [17, 18]. Transfer of EV mitochondrial components from donor to recipient cells increased recipient cellular bioenergetics and cell survival in different experimental models of disease *in vitro* and *in vivo* [17, 27-29]. Importantly, delivery of mitochondria-containing EVs into recipient cells has resulted in a variety of therapeutic responses under various pathological conditions. For instance, Silva *et al*. demonstrated that MV-mediated mitochondrial transfer into recipient pulmonary endothelial cells resulted in a three-fold increase in recipient cell ATP levels and a six-fold increase in mitochondrial respiration [30]. Our previous studies showed that human BEC cell line-derived MVs contained mitochondria [31], that upon transfer into recipient

human BECs increased cellular ATP levels, and mitochondrial respiration in normoxic and hypoxic culture conditions [31, 32]. Thus, delivery of mitochondria containing EVs is a promising treatment strategy to restore cellular bioenergetics in disorders associated with mitochondrial dysfunction.

The therapeutic efficacy of EVs depends on the source of EVs that may define its natural affinity to recipient cells and innate EV cargo. EV membranes may play a role in binding to the recipient cells and subsequent internalization into the target cells. EVs can be isolated from most eukaryotic cell types, and thus, selecting an appropriate EV donor cell type will likely influence the innate EV cargo and membrane characteristics that can ultimately determine the extent of therapeutic responses in the recipient cells. Harvesting EVs from the same type of donor cells as that of the target recipient cells may increase EV binding and internalization via "homotypic" interactions into the recipient cells. As BBB-lining BECs play a vital role in the pathophysiology of ischemic stroke, BEC-derived EVs may be an effective strategy to improve the functional integrity of recipient BECs and mitigate stroke-induced brain damage [33].

Moreover, the species of EV donor cells may contribute to the safety and efficacy of EV therapeutics in the preclinical and clinical phases of product development. Therapeutic EVs are often derived from human cell lines but are primarily tested in rodents and other animal disease models throughout preclinical development [34]. EV harvested from donor species different than the recipient species ("heterotypic" pair) may exert cross-species immunogenicity and toxicity to the recipient species and/or may compromise therapeutic efficacy [34]. Our previous pilot study administered human BEC (**hBEC**)-MVs via intravenous (**IV**) injection into a mouse middle

cerebral artery occlusion (**MCAo**) model of ischemic stroke. In the absence of treatment-related mortalities, MV-injected mice showed a trend of reduced brain infarct volume compared to vehicle-treated mice [31]. In this work, we *hypothesized* that IV-administration of mouse BEC (**mBEC**)-MV in a mouse MCAo model of stroke may exert superior therapeutic responses.

First, we isolated EXOs and MVs from mBEC and hBEC cell lines and compared their particle characteristics, morphology and protein biomarkers. Second, we demonstrated the presence of mitochondrial components in hBEC and mBEC-MVs using transmission electron microscopy (**TEM**) and western blot analysis. Third, we evaluated homotypic and heterotypic EV donor cell-recipient cell pairs (1) to compare MV mitochondrial transfer into recipient mBECs and hBECs under normoxic and OGD conditions using fluorescence microscopy and flow cytometry and (2) to determine the effect of EV exposure on recipient ischemic BEC ATP levels and mitochondrial respiration using a luminescence-based ATP and Seahorse mitochondrial function assays. Lastly, we determined the therapeutic effect of mBEC-MVs on the resulting brain infarct volume and neurological function in a mouse model of ischemic stroke. Our data demonstrated that mBEC-MVs outperformed hBEC-MVs in transferring the innate MV mitochondrial load and concurrently mitochondrial function in recipient ischemic mBEC *in vitro*. Importantly, IV-injected mBEC-MVs showed a significant reduction in mouse brain infarct volume and significantly improved neurological functions in a mouse MCAo model of ischemic stroke.

2. Materials and Methods

2.1. Materials

Material	Supplier
Endothelial cell basal medium	Lonza (Walkersville, MD)
Pierce Micro BCA and BCA protein assay kits	Thermo Scientific (Rockford, IL).
Collagen Type I	Corning (Discovery Labware Inc., Bedford, MA)
Hydrocortisone, human basic fibroblast growth factor, ascorbic acid and rotenone	Sigma-Aldrich (Saint Louis, MO)
Penicillin-Streptomycin solution, Chemically Defined Lipid Concentrate	Invitrogen (Carlsbad, CA)
Polycarbonate centrifuge tubes	Beckman Coulter, Inc. (Brea, CA)
MitoTracker Deep Red FM	Thermo Scientific (Rockford, IL)
Mouse monoclonal antibodies against ATP5A (cat#ab14748), GAPDH (cat#ab8245)	Abcam (Cambridge, MA)
Mouse monoclonal antibody against CD9 (cat#ab92726)	Life Technologies Corporation (Eugene, OR)
Alexa Fluor 790-conjugated donkey anti-mouse IgG	Jackson ImmunoResearch Lab Inc. (West Grove, PA)
Cell Titer Glo 2.0 reagent	Promega (Madison, WI)
Radioimmunoprecipitation assay buffer	Alfa Aesar (Ward Hill, MA)
Nitrocellulose membrane	GE Healthcare Life Sciences (Germany)
Intercept blocking buffer	LI-COR Inc. (Lincoln, NE)

2.2.Cell culture

A mouse cerebral endothelial cell line (bEnd.3, cat# CRL2299) was purchased from ATCC (Manassas, VA) at passage number (P) 22 and used until P32 in all the experiments. ***We refer to bEnd.3 cells as mBECs wherever applicable.*** mBECs were cultured in complete growth medium containing glutamine-supplemented Dulbecco's Modified Eagle's Medium (DMEM/high glucose + Glutamax, Gibco, Carlsbad, CA) supplemented with 10% fetal bovine serum in tissue culture flasks. Pre-warmed complete growth medium was replenished every 48 hours until cells reached 80-90% confluency. For subculturing, the cells were washed with 1*x* phosphate buffer saline (PBS) and detached from the flask using TrypLE Express (Gibco, Denmark), followed by neutralization with complete growth medium before passaging or plating.

A human cerebral microvascular brain endothelial cell line (hCMEC/D3, cat#102114.3C) was received from Cedarlane Laboratories (Burlington, Ontario) at P25 and used between P25 and P35 in all experiments [31, 32, 35]. ***We refer to hCMEC/D3 cells as hBECs wherever applicable.*** hBECs were grown in tissue culture flasks and plates pre-coated using 0.15 mg/mL rat collagen I in a humidified 5% CO_2 incubator at 37 ± 0.5˚C (Isotemp, Thermo Fisher Scientific). The cells were cultured in complete growth medium composed of endothelial cell basal medium supplemented with 5% fetal bovine serum, penicillin (100 units/mL)-streptomycin (100 µg/mL) mixture, hydrocortisone (1.4 µM), ascorbic acid (5 µg/mL), Chemically Defined Lipid Concentrate (1% v/v), 10 mM HEPES (pH 7.4), and human basic fibroblast growth factor (1 ng/mL). The complete growth medium was replenished every 48 hours until the cells formed confluent monolayers. Cells were passaged as described in the previous paragraph. Cell suspensions stained with trypan blue (1:1 v/v ratio) were counted to calculate % live cells using a

hemocytometer before passaging at 1:3 to 1:5 v/v ratios or plating in well plates at the indicated cell densities [36].

2.3. Isolation of exosomes and microvesicles from mBEC and hBEC cell lines

We studied exosomes (EXOs) and microvesicles (MVs) separately and collectively refer to EXOs and MVs as extracellular vesicles (EVs) wherever applicable. EXOs and MVs were isolated from the conditioned medium of mBECs or hBECs using the differential ultracentrifugation method described earlier [31, 35, 36]. Briefly, mBECs and hBECs were cultured in complete growth medium in tissue culture flasks with a growth area of 175 cm^2 (T175). Confluent BECs were washed with pre-warmed PBS pH 7.4 (0.0067M, PO_4) without calcium and magnesium and incubated with serum-free medium for 48 h in a humidified incubator. Post-incubation, the EV-conditioned medium was collected in polypropylene tubes and centrifuged at 300 ×g for 11 min followed by 2000 ×g for 22 min to pellet down apoptotic bodies and cell debris using an Eppendorf 5810 R 15 amp centrifuge (Eppendorf, Germany). The supernatant was transferred to polycarbonate tubes and centrifuged at 20,000 ×g for 45 min at 4°C to pellet MVs using a Sorvall MX 120+ micro-ultracentrifuge (Thermo Scientific, Santa Clara, CA). Next, the supernatant was filtered through 0.22 µm polyethersulfone filters into polycarbonate tubes and centrifuged at 120,000 ×g for 80 min to pellet EXOs. The supernatants were then discarded. MV and EXO pellets were suspended in PBS pH 7.4 and stored at -20 °C until further use. The total EV protein content was measured using a Pierce micro BCA assay kit (Thermo Scientific, Rockford, IL) as described earlier [35, 36].

For isolation of mitochondria-depleted EVs, confluent mBEC and hBECs were treated with 0.25 μM rotenone (**RTN**, mitochondrial complex I inhibitor) in complete culture medium for four hours. Post-treatment, the treatment mixture was replaced with serum-free culture medium and incubated in a humidified incubator at 37 °C for 48 h. We isolated EXOs and MVs from the conditioned medium of BECs using a differential ultracentrifugation method described above. EVs isolated post-RTN treatment were referred to as **RTN-EXOs** and **RTN-MVs**, respectively.

2.4. Dynamic light scattering

Particle diameters and zeta potential of mBEC and hBEC-EVs were measured using dynamic light scattering. EXOs and MVs were diluted to a final concentration of 0.1 mg EV protein/mL in either PBS pH 7.4 for particle diameters or in deionized water for zeta potential measurements. EV samples were analyzed using a Malvern Zetasizer Pro (Malvern Panalytical Inc., Worcestershire, UK). All samples were analyzed in triplicate measurements. Average particle diameter, dispersity index, and zeta potential values were reported as mean ± standard deviation (SD) of three independent experiments.

2.5. Nanoparticle tracking analysis

Stock samples of EVs (0.1 mg EV protein/mL) were diluted to 1:100 and 1:200 in PBS pH 7.4 and analyzed using a multiple-laser Zetaview f-NTA Nanoparticle Tracking Analyzer (Particle Metrix Inc., Mebane, NC). Prior to measurement, ZetaView was calibrated with 100 nm

polystyrene beads and three 60 s videos were acquired at 520 nm laser wavelengths for particle diameter and concentration measurements. Average EV concentrations were reported as mean ± SD of n = 3 measurements.

2.6. Transmission electron microscopy (TEM) of EVs

The morphology of negative-stained EVs and the presence of mitochondria in sectioned EVs were evaluated using the TEM described earlier [31].

Negative-stain images of EVs: EV suspensions (150 μL) were pelleted at 100,000 ×g in a Beckman Airfuge for 45 min; the supernatant was carefully removed, and the pellets were gently resuspended in 30 μL of PBS. Formvar coated, 100 mesh grids were floated onto 10 μL of this suspension and incubated for 5 min. The solution was wicked away with Whatman filter paper and stained with 0.45 μm filtered, 1% uranyl acetate. EV images were then acquired using a JEM-1400 Flash transmission electron microscope (JEOL, Peabody, 268 MA, USA) fitted with a bottom mount AMT digital camera (Danvers, MA, USA).

TEM of cross-sectioned EVs: EV suspensions were pelleted at 100,000 ×g in a Beckman airfuge for 20 min, and the pellets were fixed in 2.5% glutaraldehyde in PBS overnight. The supernatant was removed, and the cell pellets were washed 3× in PBS and post-fixed in 1% OsO4, 1% $K_3Fe(CN)_6$ for one hour. Following three additional PBS washes, the pellet was dehydrated through a graded series of 30–100% ethanol. After several changes of 100% resin over 24 h, the pellet was embedded in a final change of resin, cured at 37 ºC overnight, followed

by additional hardening at 65 ºC for two more days. Ultrathin (70 nm) sections were collected on 200 mesh copper grids and stained with 2% uranyl acetate in 50% methanol for 10 min, followed by 1% lead citrate for seven min. Sections were imaged using a JEOL JEM 1400 Plus transmission electron microscope (Peabody, MA) at 80 kV fitted with a side mount AMT 2 k digital camera (Advanced Microscopy Techniques, Danvers, MA).

2.7. Western blot analysis

mBEC and hBEC-EVs were evaluated for characteristic protein biomarkers using western blotting. BEC lysates were used as positive controls. BEC lysate (10 µg) and 50 µg EV proteins were mixed with laemmli sodium dodecyl sulfate sample buffer and denatured at 95°C for 5 min. The samples were loaded onto a 4% stacking and 10% resolving polyacrylamide gel. Premixed molecular weight markers (Protein standards, ladder, 250 kDa - 10 kDa, cat#1610374, BioRad Laboratories Inc.) were used as a reference control to confirm molecular masses of the protein bands in the sample lanes. The gel was run at 120 V for 120 min in Tris-Glycine pH 8.8 running buffer using a PowerPac Basic setup gel electrophoresis assembly (BioRad Laboratories Inc.). The proteins were transferred onto a 0.45 µm nitrocellulose membrane at 75 V for 90 min using a transfer assembly (BioRad Laboratories Inc.). The membrane was washed with 0.1% Tween 20 containing Tris-buffered saline pH 7.4 (T-TBS) and blocked with Intercept blocking buffer solution (LI-COR Inc., Lincoln, NE) for one hour at room temperature. The membrane was incubated with mouse anti-GAPDH (1 µg/mL), mouse anti-ATP5A (1 µg/mL), rabbit anti-TOMM20 (1 µg/mL), rabbit anti-calnexin (1 µg/mL), rabbit anti-CD9 (0.2 µg/mL), rabbit anti-CD63 (1/1000 dilution) and rabbit anti-ARF-6 (1 µg/mL) primary antibodies in blocking buffer and T-TBS solution (1:1::v/v) overnight at 4°C. The membrane was washed with T-TBS and

incubated with anti-mouse or anti-rabbit AF790 secondary antibodies (0.05 μg/mL) for one hour at room temperature. The membrane was washed with T-TBS and scanned using an Odyssey M imager (LI-COR Inc., Lincoln, NE) imager at 700 and 800 nm channels.

2.8. MV mitochondria transfer into recipient BECs

2.8.1. Isolation of mitochondria-labeled EVs

For labelling EV mitochondria, EXOs and MVs were isolated from mBECs and hBECs prestained with Mitotracker deep red (**MitoT-red**). Confluent mBECs and hBECs in T175 flasks were stained with 100 nM MitoT-red in serum-free medium for 30 minutes in a humidified incubator. Post-incubation, the old medium was removed, and cells were washed with PBS pH 7.4. The cells were incubated in serum-free medium for 48 hours in a humidified incubator. Post-incubation, the conditioned medium was collected in polypropylene tubes. MitoT-red-MVs and MitoT-red-EXOs were isolated using the differential ultracentrifugation method described in ***section 2.3.*** The total protein content in MitoT-red-EVs was determined using a MicroBCA assay.

2.8.2. Uptake of MitoT-red-EV into recipient mBECs and hBECs using fluorescence microscopy

EV mitochondria transfer into recipient BECs under normoxic conditions was studied using fluorescence microscopy. Recipient mBECs and hBECs were cultured in 24-well tissue culture

plates at 100,000 cells/well in complete growth medium for 72 hours. The cells were treated with mBEC and hBEC-derived MitoT-red-EVs at 10, 30, and 60 μg EV protein/well in complete growth medium for 48 hours in a humidified incubator. Untreated cells incubated with complete growth medium were used as a control. Post-incubation, the treatment mixture was removed, and cells were washed with PBS. Cells were incubated with Hoechst stain (1 μg/mL) for 15 min. Cells treated with MitoT-red dye (100 nM for 30 min) were used as a positive control for MitoT-red signal detection. The cells were incubated in phenol red-free DMEM with 10% FBS medium prior to observation under an Olympus IX 73 epifluorescent inverted microscope (Olympus, Pittsburgh, PA) using Cyanine-5 (Cy5, excitation 651 nm and emission 670 nm) and DAPI channels at 20*x* magnification. Images were acquired and analyzed using CellSens Dimension software (Olympus, Pittsburgh, PA). The total sum of grayscale signal intensities in the Cy5 channel was used for signal quantification. The signal intensities of the untreated control group (background) were subtracted from signal intensities of the treated groups.

2.8.3. Quantitative analysis of MitoT-red-EV mitochondria transfer into recipient mBECs and hBECs under normoxic and hypoxic conditions using flow cytometry

Recipient mBECs and hBECs were cultured in 24-well plates at 100,000 cells/well in complete growth medium. For normoxic conditions, confluent cells were treated with MitoT-red-EXOs and MitoT-red-MV at 10, 30, and 60 μg EV protein/well in complete growth medium for 24 h in a humidified incubator. For OGD conditions, confluent cells were treated with MitoT-red-EXOs and MitoT-red-MV at 10, 30, and 60 μg EV protein/well in oxygen-glucose deprived (**OGD**) medium in a hypoxia chamber (Billups Rothenberg, Del Mar, CA) pre-flushed with 5%

carbon dioxide, 5% hydrogen and 90% nitrogen at 37±0.5˚C for 24 h. The OGD medium [37] was composed of: 120 mM NaCl, 5.4 mM KCl, 1.8 mM $CaCl_2$, 0.8 mM $MgCl_2$, 25 mM Tris-HCl, pH 7.4. Unstained and untreated cells were used as a control. Post-treatment, the cells were washed with PBS, dissociated using TrypLE Express, diluted with PBS containing 1% FBS, and collected into centrifuge tubes. For each sample, an aliquot of a 100 μL cell suspension was analyzed through an Attune NxT Flow cytometer and 10,000 events were recorded in FSC *vs*. SSC plots. Mitotracker deep red fluorescence intensity was detected at 670/14 nm, and percentage signal intensities were analyzed in histogram plots generated using Attune 3.2.3 software. Mitotracker background signals were gated using the controls, including PBS and untreated cells.

2.9. Effect of EV treatment on relative ATP levels in the oxygen glucose-deprived recipient BECs

The effect of mBEC and hBEC-EVs on the relative cellular ATP levels in the recipient mBECs and hBECs under OGD conditions was measured using a Cell Titer Glo-based ATP assay. mBECs and hBECs in complete growth medium were cultured at 16,500 cells per well in a 96-well plate. The cells were incubated in a humidified incubator at 37°C for 72 h. Post-incubation, the cells were washed with PBS pH 7.4 and treated with OGD medium for four hours in an OGD chamber pre-flushed with 5% carbon dioxide, 5% hydrogen and 90% nitrogen at 37±0.5˚C. Post-incubation, the OGD medium was removed, and cells were treated with mBEC- and hBEC-EVs diluted at different concentrations in the OGD medium for 24 h. Cells treated

with OGD medium alone were used as OGD control, and cells treated with complete growth medium were used as normoxic control. After incubation, the treatment mixture was removed, and cells were washed and incubated with complete growth medium. An equal volume of Cell titer glo reagent was added. The plate was incubated for 15 min on a mechanical orbital shaker. A 60 µL aliquot of the mixture was transferred to a white opaque plate, and relative luminescence units at 1 s integration time were measured using a plate reader (Synergy HTX multimode plate reader, BioTek Inc., Winooski, VT). Relative ATP levels were calculated by normalizing the relative luminescence units (RLU) of treatment groups to the RLU of control, untreated cells.

We evaluated the effect of EVs isolated from donor cells with impaired mitochondrial complex I function on recipient BEC ATP levels. To inhibit mitochondrial function, EVs were isolated from the conditioned medium of mBECs and hBECs pretreated with 0.25 µM RTN, henceforth referred to as RTN-EXOs and RTN-MVs. Confluent mBECs and hBECs in 96-well plates were treated with OGD medium for four hours in an OGD chamber pre-flushed with 5% carbon dioxide, 5% hydrogen and 90% nitrogen at 37±0.5˚C. Post-incubation, the OGD medium was removed, and the cells were incubated with naïve EXOs, MVs, RTN-EXOs, and RTN-MVs-isolated from mBEC and hBECs at 10 µg EV protein/well under OGD conditions. Normoxic BECs treated with complete culture medium and cells treated with OGD medium (OGD untreated cells) were used as controls. After incubation, the treatment mixture was removed, and the ATP assay was performed, as described in the paragraph above.

2.10. Measurement of mitochondrial function using Seahorse analysis

The mitochondrial function of recipient mBECs treated with EVs during OGD conditions were evaluated using the Seahorse analysis by measuring oxygen consumption (**OCR**) [32, 38]. mBECs seeded at 20,000 cells/well were cultured in a Seahorse XF96 plate for three days. Post-incubation, the cells were washed with PBS pH 7.4 and treated with OGD medium for four hours in a hypoxic chamber. The cells were incubated with mBEC and hBEC-derived EXOs and MVs at different EV concentrations in OGD medium for 24 h. Post-incubation, the medium was replaced with pre-warmed DMEM and used for Seahorse analysis. After measurement of baseline OCR, 2.5 μmol/L oligomycin A and 0.7 μmol/L carbonyl cyanide-p-trifluoromethoxyphenyl-hydrazone were consecutively added to measure the proton leak and maximal OCR, respectively [38]. The total protein content of the cells in each well was measured using a Pierce BCA assay.

2.11. *In vivo* studies

2.11.1. *Mice*

Young male C57BL/6 mice (8–12 weeks) were purchased from Jackson laboratories. Mice were acclimated in our animal facilities for one week before use. Mice were housed 4–5 per cage, with a 12-h light/dark schedule in a temperature and humidity-controlled vivarium, with *ad-libitum* access to a pelleted rodent diet (irradiated LabDiet 5053, PicoLab rodent diet 20) and filtered water. All experiments were approved by the Institutional Animal Care and Use Committee at the University of Texas Health Science Center, Houston. This study was

performed in accordance with the guidelines provided by the National Institute of Health and followed RIGOR guidelines. Only male animals were used in this study to allow comparisons to earlier studies [31] and to exclude potential sex and estrogen-related effects. Animals were randomly assigned to treatment groups.

2.11.2. Mouse middle cerebral artery occlusion stroke model

Focal transient cerebral ischemia was induced in mice by right middle cerebral artery occlusion (**MCAo**) followed by reperfusion as described previously [39, 40]. Briefly, young (3-month) male C57BL/6 mice were initially placed and anaesthetized in a chamber with 4% isoflurane, and adequate sedation was confirmed by tail pinch for all surgical procedures. Surgeries were performed under 1–2% continuous isoflurane. A 90-minute MCAo was achieved by blocking blood flow to MCA using a silicone-coated filament via the external carotid artery. At the end of ischemia (90 min MCAo), mice were briefly re-anesthetized, and reperfusion was initiated by filament withdrawal. Body temperature was maintained by placing the mouse on a heating pad at ~37 ◦C during surgical procedures. Two hours after stroke onset, mice were randomly assigned to receive 100 μg of mBEC-MVs in 200 μL PBS (n=7) or vehicle (PBS, n=8) treatment by intravenous tail vein injection. Sample size was determined using power analysis based on results from the initial cohort [31]. Mice were euthanized 24 h after the stroke, and brains were analyzed for infarct size using 2,3,5-triphenyl tetrazolium chloride (**TTC**)-stained sections. Infarct analysis was performed by an investigator blinded to the treatment groups.

2.11.3. Neurological Deficit Scoring (NDS)

The behavioral functions of MCAo mice was examined by a blinded investigator using the Neurological Deficit Score (NDS) at 24 h after stroke. We used our standard graded scoring system to get NDS as follows: 0 = no deficit; 1 = forelimb weakness and torso turning to the ipsilateral side when held by the tail; 2 = circling to affected side; 3 = unable to bear weight on affected side; and 4 = no spontaneous locomotor activity or barrel rolling, as previously described [41-45].

2.12. Statistical analysis

Statistically significant differences between the means of controls and treatment groups or within treatment groups were determined using one-way or two-way analysis of variance (ANOVA) with post hoc corrections using multiple comparison tests at $\alpha=0.05$ using GraphPad Prism 10 (GraphPad Software). Mann–Whitney U test was used for ordinal data (i.e., NDS) analysis. The notations for the different significance levels are indicated as follows: $*p < 0.05$, $**p < 0.01$, $***p < 0.001$, $****p < 0.0001$.

3. Results

3.1. Physicochemical characterization of mouse and human BEC-derived EVs

We used b.End3 and hCMEC/D3 cells as models of mouse (**mBEC**) and human BECs (**hBEC**), respectively. We compared mBEC- *vs.* hBEC-EVs in terms of their physicochemical characteristics, morphology, and EV biomarkers. Average particle diameters of mBEC EXOs and MVs were 167 nm and 442 nm, with characteristic negative zeta potentials of about -25.1 mV and -27.5 mV, respectively (**Fig. 1a**). hBEC-EXOs and MVs showed average particle diameters of 137 nm and 214 nm with average zeta potentials of -13.4 mV and -24.3 mV, respectively (**Fig. 1a**). For both cell lines, MVs showed significantly greater particle sizes than EXOs, and there was no significant difference between the average particle diameters of mBEC and hBEC-EXOs. However, mBEC-MVs showed significantly greater particle diameters compared to hBEC-MVs. Notably, mBECs secreted EVs at lower concentrations of about 5.1×10^{7} particles/mL EXOs and 2.8×10^{8} particles/mL MVs (**Fig. 1a**). In contrast, hBEC secreted about 2.1×10^{9} particles/mL EXOs and 1.7×10^{9} particles/mL MVs (**Fig. 1a**). Representative TEM images of negatively-stained EVs derived from both cell lines showed that EXOs were <200 nm and MVs were >200 nm with heterogenous shapes (**Fig. 1b**). The observed morphologies are consistent with TEM images of EVs in the published literature [46, 47].

a. Physicochemical characterization of BEC-EVs

	mBEC-EVs		hBEC-EVs	
	EXOs	MVs	EXOs	MVs
Particle diameters (nm)	167.4 ± 21.8	441.9 ± 48.4	137.4 ± 26.3	213.9 ± 33.8
Dispersity index	0.4 ± 0.1	0.5 ± 0.1	0.3 ± 0.1	0.4 ± 0.0
Zeta potential (mV)	-25.1 ± 2.2	-27.5 ± 5.4	-13.4 ± 1.2	-24.3 ± 2.4
Particle concentraion (EV particles/mL)	$5.1 \pm 0.9\times10^{7}$	$2.8 \pm 0.8\times10^{8}$	$2.1 \pm 0.9\times10^{9}$	$1.7 \pm 0.2\times10^{9}$

b. TEM images of negatively-stained EVs

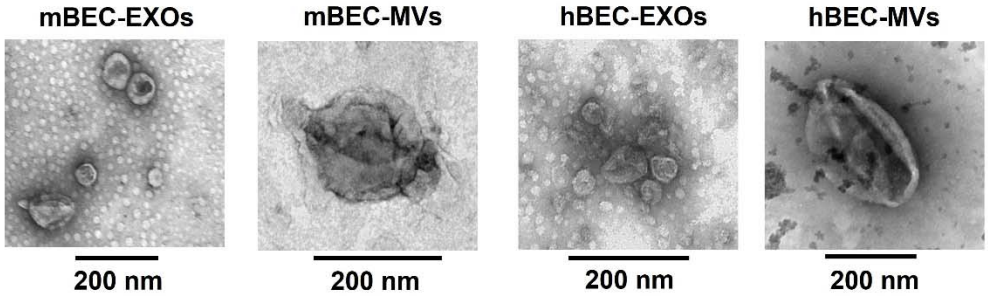

c. Protein-based characterization of BEC-EVs

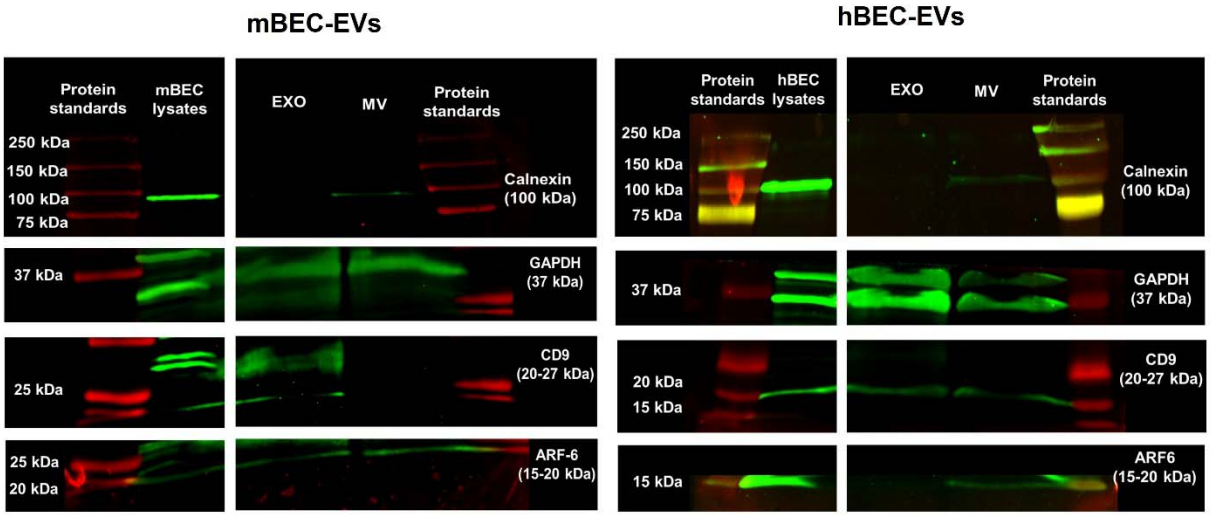

Figure 1: Physicochemical characterization of mBEC and hBEC-EVs. a) *Dynamic light scattering and nanoparticle tracking analysis (NTA) of mBEC and hBEC-EXOs and MVs.* Freshly isolated EXOs and MVs were diluted to 0.1 mg EV protein/mL in 1*x* PBS pH 7.4 for particle diameters and NTA. The samples were diluted in deionized water for zeta potential measurements. Dynamic light scattering analysis of EVs was conducted on Malvern Zetasizer Pro-Red (Malvern Panalytical), and EV particle concentrations were measured on a multiple-laser ZetaView f-NTA Nanoparticle Tracking Analyzer (Particle Metrix Inc., Mebane, NC). DLS data are presented as mean ± SD of n = 3 independent experiments, and NTA data are presented as mean ± SD of n=3 measurements. **(b)** *Morphology of EVs.* Representative negative stain transmission electron microscopy (TEM) images of mBEC and hBEC-EVs. Scale bar: 200 nm. **(c)** *Detection of membrane and luminal biomarkers of mBEC and hBEC-derived EVs*

using western blot analysis. Western blot shows the relative expression of calnexin (100 kDa), glyceraldehyde 3-phosphate dehydrogenase (GAPDH, 37 kDa), CD9 (20-27 kDa), and ARF6 (15-20 kDa) in EXOs and MVs. Cell lysates were used as a control, and protein standards were used as a reference for the molecular weight of protein bands. Cell lysates (15 μg) and EV lysates (50 μg) mixed with laemmli sample buffer were electrophoresed on a sodium dodecyl sulfate-polyacrylamide gel. The proteins were transferred onto a nitrocellulose membrane, and non-specific proteins were blocked using a blocking buffer. The blot was incubated with primary antibodies overnight at 4 °C and subsequently incubated with secondary antibodies at room temperature. The blots were imaged on the 700 and 800 nm channels using an Odyssey M imager (LI-COR Inc. Lincoln, NE) and processed using ImageStudio 5.2 software.

We compared membrane and luminal biomarker proteins in mBEC *vs*. hBEC-EVs using western blot analysis. According to the Minimal Information for Studies of Extracellular Vesicles (MISEV) 2018 guidelines, protein content-based characterization of EVs should demonstrate the purity and characteristic proteins associated with EV subtypes. We performed western blot analysis of mBEC and hBEC-EXOs and MVs to evaluate the relative expression of calnexin (to demonstrate that EVs are free of endoplasmic reticulum contaminants), tetraspanin CD9 and CD63 (transmembrane proteins associated with the plasma membrane or endosome), and glyceraldehyde 3-phosphate dehydrogenase (GAPDH as a model cytosolic protein recovered in EVs). mBEC and hBEC cell lysates showed bands of all the above proteins at their characteristic molecular masses (**Fig. 1c**), suggesting the suitability of western blotting for detecting these biomarker proteins and their relative abundance in the donor BECs. First, calnexin (endoplasmic reticulum marker, 100 kDa) was used to determine whether isolated EV samples contained cellular contaminants or non-EV co-isolated structures. mBEC- and hBEC-EXOs showed no calnexin expression, suggesting that isolated EXOs were free from endoplasmic reticulum contaminants. In contrast, faint expression of calnexin in MVs (**Fig. 1c**) indicated minimal endoplasmic reticulum impurities in the isolated MVs. Second, mouse and human BEC-EXOs and MVs expressed GAPDH, suggesting the incorporation of soluble

cytosolic proteins in EVs during their biogenesis. Third, tetraspanin CD9 (20-27 kDa) was selectively present in mBEC-EXOs, whereas mBEC-MVs did not show the CD9 band (**Fig. 1c**). Notably, CD9 was detected in both hBEC-EXOs and MVs. Lastly, mBEC and hBEC-MVs showed adenosine diphosphate-ribosomal factor (ARF6) expression at its characteristic molecular weight of 15-20 kDa. In contrast, mBEC-EXOs showed a faint band, and hBEC-EXOs did not show any ARF6 band (**Fig. 1c**), suggesting that ARF6 is selectively expressed in MVs and is a biomarker for mBEC and hBEC-MVs.

3.2. Mouse and human BEC-MVs contained mitochondria and mitochondrial proteins

We acquired TEM images of cross-sectioned EXOs and MVs isolated from mBEC and hBECs (**Fig. 2a**). The yellow arrowheads point to EXO membranes, the blue arrowhead indicates MV membranes and the maroon arrowheads point to MV mitochondria. Mitochondria were detected as membrane-bound electron-dense structures in the MV lumen. Representative TEM images showed that mBEC- and hBEC-MVs (blue arrows, **Fig. 2a**) contained a couple of mitochondria (maroon arrows) with varying sizes and morphologies in the MV lumen. In contrast, EXO lumen lacked electron-dense structures, suggesting the absence of mitochondria in mBEC and hBEC-EXOs. It is important to note that the morphology of MV mitochondria in our TEM images was comparable with extracellular free mitochondria or mitochondria-containing EVs presented in previously published reports [16, 18, 48]. So, we conclude that irrespective of the donor cell species, both mBEC and hBEC-MVs contained mitochondria, and EXOs lacked mitochondria.

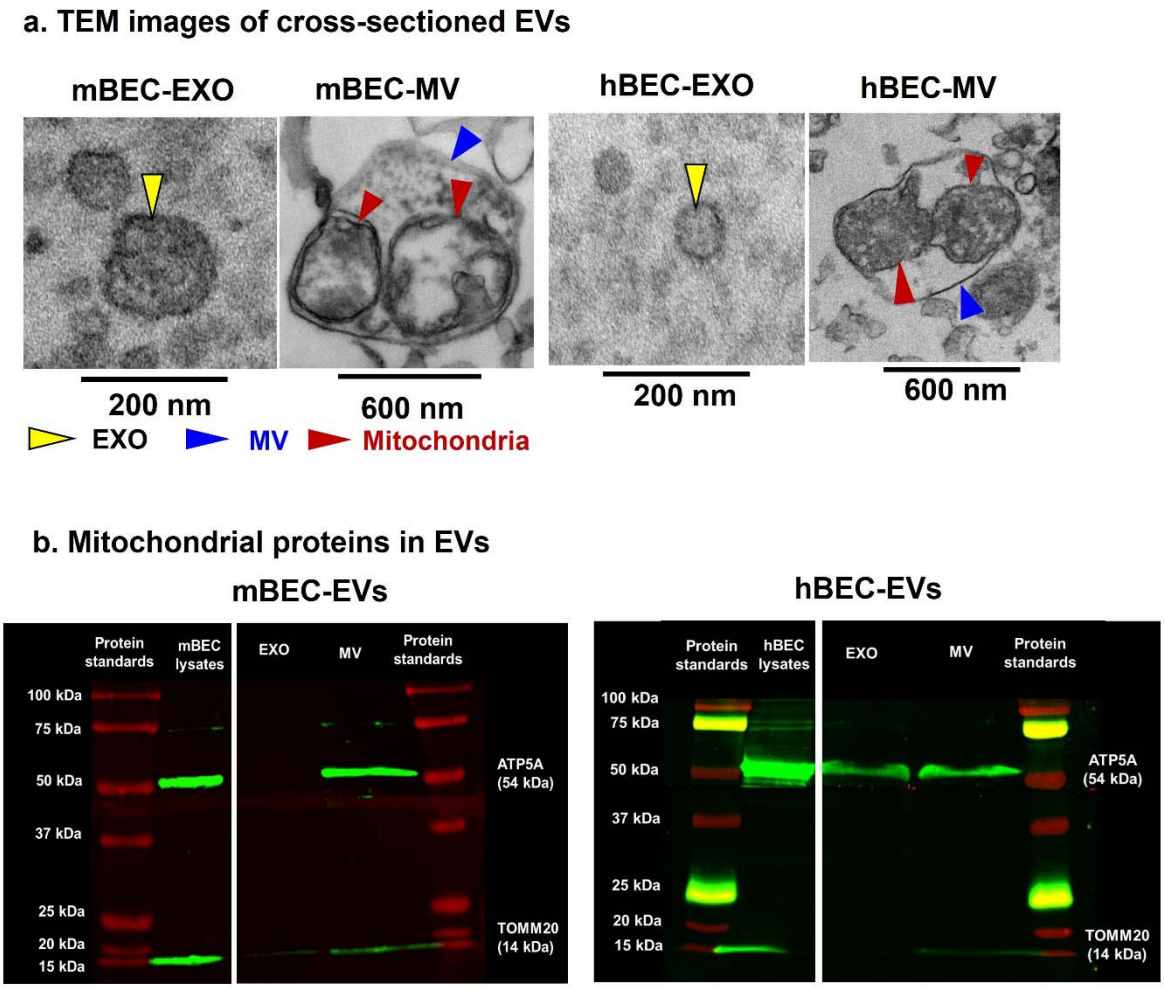

Figure 2: Selective presence of mitochondria in MVs. (**a**) *Representative TEM images of sectioned mBEC and hBEC-EXOs and -MVs.* mBEC- and hBEC-MVs (blue arrow) contained a couple of mitochondria (electron-dense structures, maroon arrows) in the MV lumen. EXO (yellow arrows)-derived from both cell lines lacked electron-dense structures in the lumen. (**b**) *Detection of mitochondrial proteins in mBEC- and hBEC-EVs using western blot analysis.* Western blots show the relative expression of ATP5A (54 kDa) and TOMM20 (14 kDa) in EXOs and MVs. Cell lysates were used as a control, and protein standards were used as a reference for the molecular mass of protein bands. The blots were imaged on the 700 and 800 nm channels using an Odyssey M imager (LI-COR Inc. Lincoln, NE) and processed using ImageStudio 5.2 software.

We further evaluated if structural and functional mitochondrial proteins are expressed in EXOs and MVs using western blot analysis. Mouse and human BEC-EXOs and MVs were analyzed for the expression of ATP5A (a subunit of electron transport chain ATP synthase, 60 kDa) and TOMM20 (translocase of the outer mitochondrial membrane complex subunit 20, 14

kDa). While mBEC-MVs showed the presence of ATP5A and TOMM20 at their characteristic molecular masses, EXOs did not show any mitochondrial protein bands (**Fig. 2b**). The selective presence of mitochondrial proteins in MVs but not in EXOs aligned with the TEM images of sectioned mBEC-MVs showing mitochondria in MVs (**Fig. 2a**). Besides, ATP5A was detected in both EXOs and MVs derived from hBECs. Importantly, TOMM20 was selectively present in hBEC-MVs (**Fig. 2b**), whereas EXOs showed no bands at the characteristic molecular mass of 14 kDa. It is likely that while both hBEC-EXOs and MVs contained functional mitochondrial proteins (ATP5A), and mitochondrial structural components (TOMM20) were selectively present in MVs, aligning with the TEM images of sectioned hBEC-MVs showing mitochondria (**Fig. 2a**).

3.3. Mouse BEC-MVs transferred mitochondria into recipient mouse and human BECs

We sought to determine whether mBEC-MVs can transfer their innate mitochondria into recipient hBECs and *vice versa* (i.e., if hBEC-MVs can transfer their innate mitochondria into recipient mBECs) using fluorescent microscopy. Mitochondria-labelled EVs were isolated from donor mBECs and hBECs-prestained using Mitotracker Red (**MitoT-red-EVs**). Subsequently, recipient mBECs and hBECs were incubated with MitoT-red-EVs at different doses, and we detected MitoT-red signals 48 h-post exposure using a fluorescence microscope. MitoT-red is a mitochondrial membrane potential dye that stains polarized (functional) mitochondria in donor cells. Untreated mBECs and hBECs showed no signals in the Cy5 channel. Cells stained with MitoT-red showed intracellular purple fluorescence signals (**Fig. 3a-b**), suggesting minimal background and specificity of MitoT-red signal detection under the Cy5 channel. mBEC- and

hBEC-derived MitoT-red-EXOs showed no signals at 10 and 30 μg doses in recipient mBECs and hBECs, whereas MitoT-red-EXOs at 60 μg showed faint intracellular MitoT-red signals (**Fig. 3a-b**). The data suggests that EXOs likely contain minimal mitochondrial load and show signs of low transfer at higher doses. The quantitative analysis of MitoT-red signals (**Fig. 3c-d**) showed that mBEC-EXOs showed a dose-dependent gradual increase in MitoT-red signals in recipient mBECs, whereas increasing the dose of hBEC-EXOs did not increase MitoT-red signals. Notably, mBEC-EXOs showed relatively higher MitoT-red signals (**Fig. 3c-d**), suggesting mBEC-EXOs likely contain a greater mitochondrial load than hBEC-EXOs.

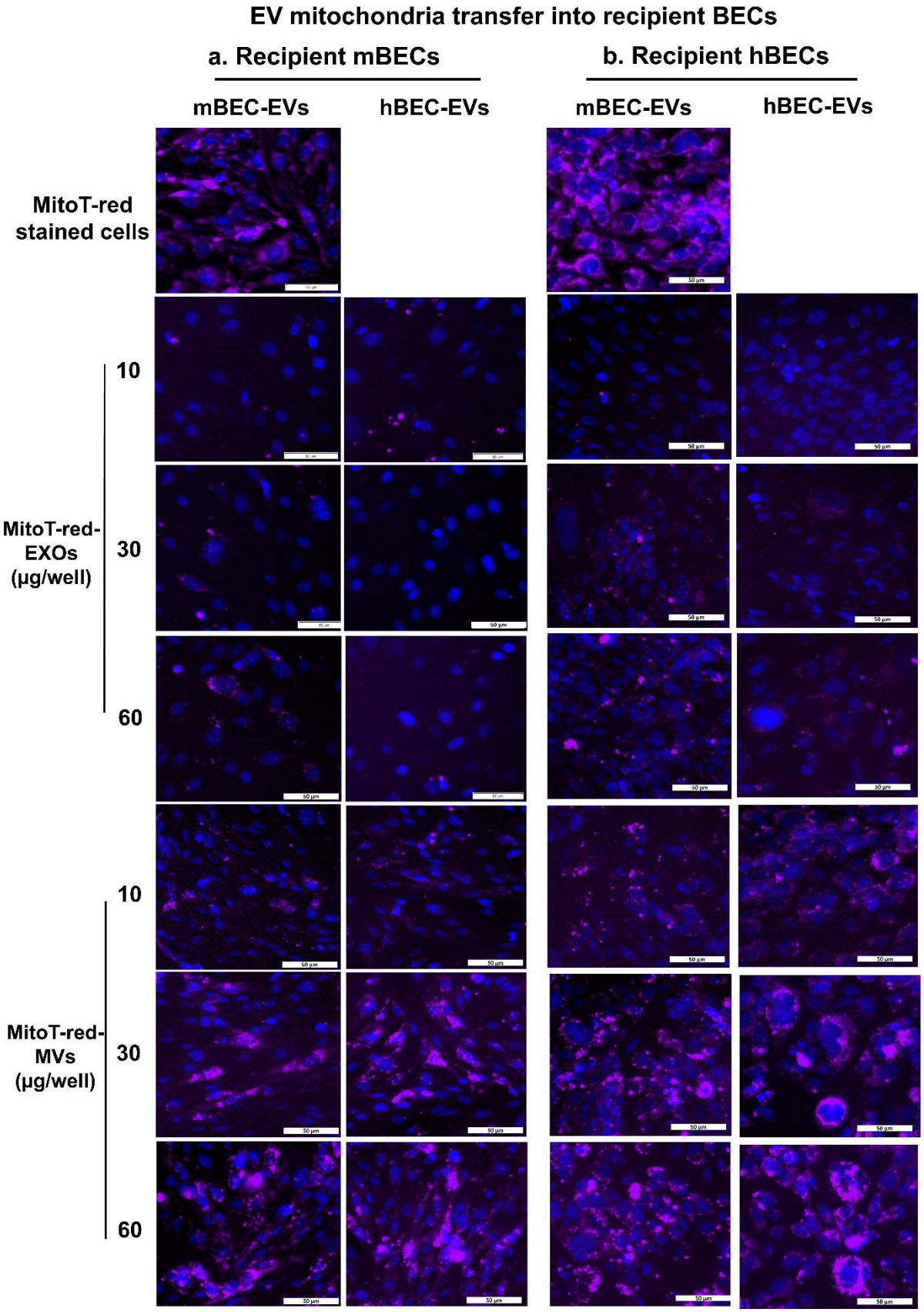
EV mitochondria transfer into recipient BECs
a. Recipient mBECs
b. Recipient hBECs
mBEC-EVs
hBEC-EVs
mBEC-EVs
hBEC-EVs
MitoT-red stained cells
MitoT-red-EXOs (µg/well)
10
30
60
MitoT-red-MVs (µg/well)
10
30
60

Figure 3a-b: MV-mediated mitochondria transfer into the recipient BECs at varying doses. mBECs and hBECs were cultured in 48-well plates in a humidified incubator at 37 °C. Recipient mBECs (**a**) and hBECs (**b**) were incubated with indicated amounts of mBEC and hBEC-derived MitoT-red-EXOs and MVs diluted in complete growth medium for 48 h. Cells treated with complete growth medium were used as control, untreated cells. Cells treated with 100 nM MitoT-red for 30 min were used as a positive control for MitoT-red signal detection under a fluorescence microscope. Post-incubation, the cells were washed and incubated with the phenol-red medium. MitoT-red signals (purple puncta) and nucleus (blue) were observed under an Olympus IX 73 epifluorescent inverted microscope using Cy5 (pseudo purple colored for mitochondria) and DAPI (pseudo blue colored for nucleus) channels at 20× magnification—scale bar 50 μm.

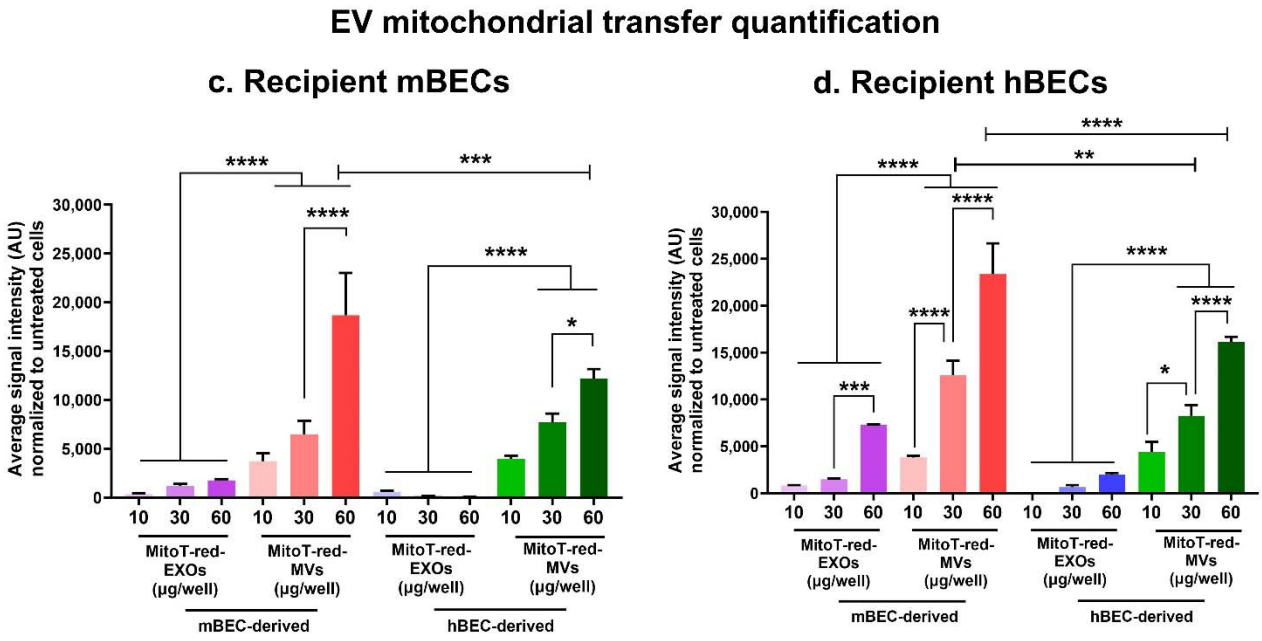

Figure 3c-d: Quantification of MV mitochondria transfer in recipient BECs. mBECs (**c**) and hBECs (**d**) were treated with mBEC and hBEC-derived MitoT-red-EXOs and MVs at indicated doses in complete growth medium for 48 h. Post-incubation, at least three images were acquired from each treatment group using an Olympus IX 73 epifluorescent inverted microscope. The total sum of grayscale signal intensities in the Cy5 channel was estimated using Olympus CellSens software. The signal intensities of the untreated control group (background) were subtracted from the signal intensities of the treatment groups. Data are presented as mean ± SD (n=3 images per treatment group). The statistically significant difference between treatment groups was analyzed using a one-way analysis of variance followed by post hoc Tukey's multiple comparison test using GraphPad Prism 10. *$p < 0.05$, **$p < 0.01$, ***$p < 0.001$, ****$p < 0.0001$.

Recipient mBECs and hBECs treated with mBEC- and hBEC-derived MitoT-red-MVs at 10 μg showed strong intracellular MitoT-red signals (**Fig. 3a-b**). Greater doses (30 and 60 μg EV protein/well) of MitoT-red-MVs showed significantly higher intracellular MitoT-red signals in both recipient mBECs and hBECs (**Fig. 3a-b**). Importantly, quantitative analysis of MitoT-red signals showed that recipient BECs treated with MVs at a dose as low as 10 μg led to a considerably greater extent of mitochondria transfer than the maximum dose of EXOs (**Fig. 3c-d**), suggesting a significantly greater mitochondrial load in MVs than EXOs. Moreover, increasing MV doses showed a dose-dependent and statistically significant ($p<0.0001$) increase in recipient BEC signals (**Fig. 3c-d)**. Notably, there was no statistically significant difference between mBEC and hBEC-MV-mediated mitochondria transfer at the low and medium MV doses in both recipient BECs. However, at higher doses, mBEC-MVs showed a significantly greater mitochondria transfer than hBEC-MVs in both recipient BECs (**Fig. 3c-d**), likely because of a greater mitochondrial load in mBEC-MVs than hBEC-MVs.

Next, we used flow cytometry to analyze MV mitochondria transfer into recipient BECs and determine whether ischemic conditions can affect MV mitochondria transfer into oxygen-glucose-deprived (**OGD**) recipient BECs. First, recipient mBECs and hBECs were treated under normoxic conditions with 10, 30, and 60 μg of MitoT-red-EVs derived from mBECs or hBECs for 24 h (**Fig. 4a-d**). Recipient mBECs treated with different doses of mBEC-derived MitoT-red-EXOs and MVs showed a dose-dependent, statistically significant ($p<0.0001$) increase in MitoT-red positive cells (**Fig. 4a**). Consistent with microscopy studies (**Fig. 3c-d**), MV-treated BECs showed significantly ($p<0.0001$) higher MitoT-red positive cells than EXO-treated cells (**Fig. 4a**). Similarly, recipient mBECs treated with hBEC-derived MitoT-red-EVs (**Fig. 4b**) and

recipient hBECs treated with mBEC- (**Fig. 4c**) as well as hBEC-derived MitoT-red-EVs (**Fig. 4d**) showed (1) a dose-dependent increase in MitoT-red positive cells, and (2) significantly greater extent of mitochondria transfer from MVs than EXOs. Importantly, recipient mBECs treated with mBEC-derived MitoT-red-EVs under OGD conditions showed a dose-dependent, significant ($p<0.0001$) increase in MitoT-red positive cells (**Fig. 4a**), suggesting that MV mitochondria were internalized by ischemic BECs. However, recipient mBECs treated with MitoT-red-EVs showed significantly ($p<0.0001$) reduced MitoT-red positive cells under OGD conditions compared to normoxic cells treated at the same dose (**Fig. 4a**), suggesting that OGD reduces BEC efficiency to internalize EV mitochondria than normoxic conditions. Notably, at the highest treated dose, the homotypic MV donor-recipient BEC pair (**Fig. 4a** and **c**) did not show any significant difference in percentage MitoT +ve cells between normoxic and OGD conditions, likely due to saturation of MV mitochondria transfer into recipient normoxic BECs at the highest tested dose. The OGD-mediated reduction in EV mitochondria uptake in BECs compared to normoxic conditions was consistent in mouse and human recipient BECs, irrespective of the EV source species (**Fig. 4b-d**).

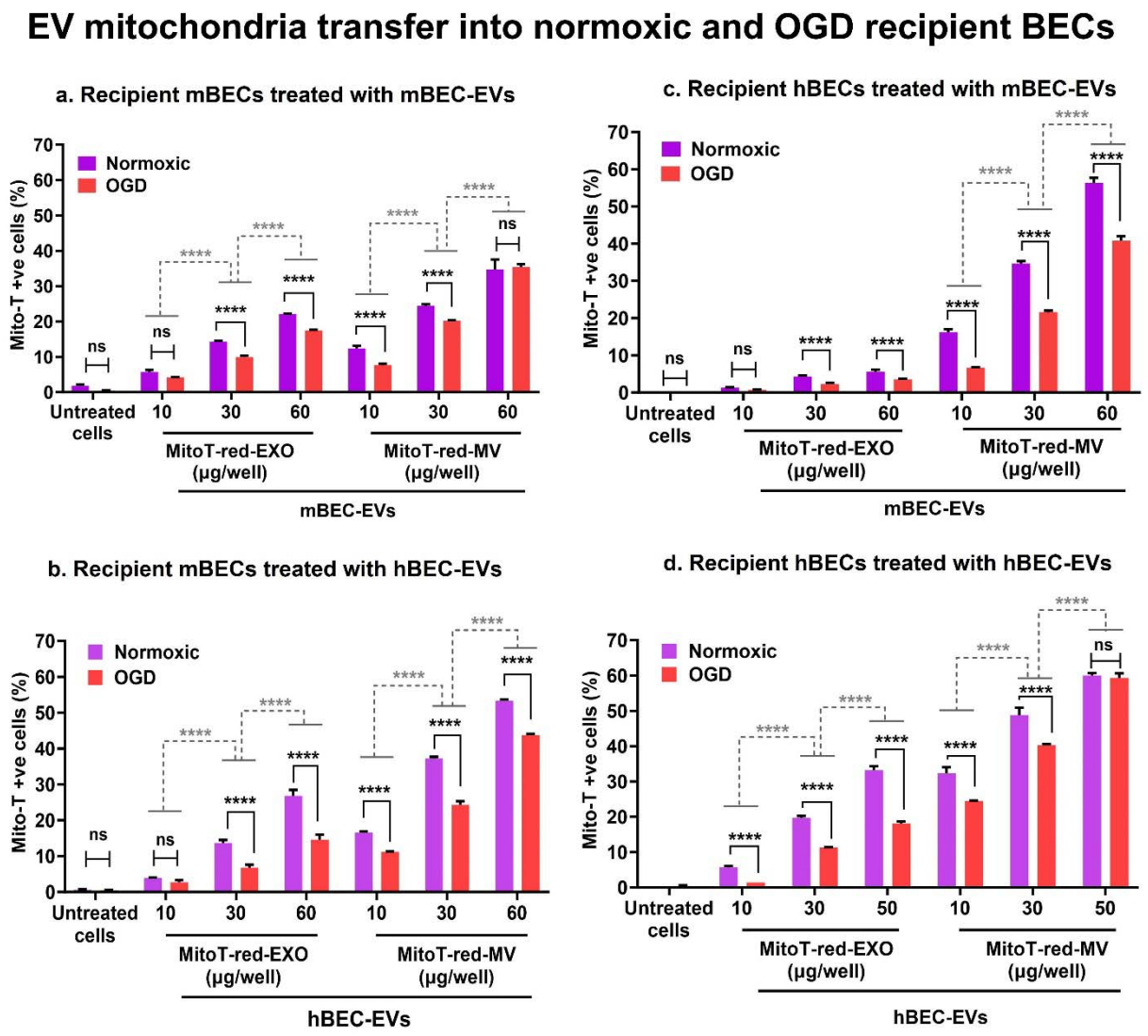

Figure 4: Transfer of EV mitochondria into recipient BECs at varying doses. Confluent mBECs and hBECs were incubated with the indicated amounts of mBEC and hBEC-derived MitoT-red-EXOs and MVs under normoxic and OGD conditions for 24 h. Post-incubation, the cells were washed, collected, and run through an Attune NxT flow cytometer. The histograms of mBECs and hBECs treated at indicated doses of MitoT-red-EVs were collected using a 674/10-nm side scatter filter in the Attune flow cytometer. Untreated and unstained BECs were used as controls to gate the background signals in histograms. MitoT-red-stained BECs were used as a positive control to gate the histograms for MitoT-red-positive counts. Subsequently, this gate was applied to quantify the percentage of MitoT-red BECs treated with MitoT-red-EVs. The percentage of maximum signal intensities of mBECs treated with mBEC-EVs (**a**), mBECs treated with hBEC-EVs (**b**), hBECs treated with mBEC-EVs (**c**), and hBECs treated with hBEC-EVs (**d**), were compared under normoxic and hypoxic conditions. Data represent mean ± SD of n = 3. The statistically significance between treatment groups was analyzed using one-way ANOVA followed by post hoc Tukey's multiple comparison test using GraphPad Prism 10. *$p < 0.05$, **$p < 0.01$, ***$p < 0.001$, ****$p < 0.0001$.

3.4. Mouse BEC-MVs outperformed human BEC-MVs in increasing recipient ischemic mouse and human BEC ATP levels

We compared the effects of mBEC and hBEC-derived EVs on the resulting ATP levels in recipient OGD BECs (**Fig. 5**). We determined whether homotypic EVs derived from the same species as the recipient cell (**Fig. 5a,d**) may show higher functional efficiency than heterotypic pairs: cross-species EVs and recipient cells (**Fig. 5b,c**). Recipient mBECs and hBECs were incubated in OGD medium in a hypoxic chamber for four hours. OGD-exposed BECs were treated with hBEC- and mBEC-EVs at different concentrations for 24 h. Post-exposure, recipient BEC relative ATP levels were measured using a Cell TiterGlo-based luminescent ATP assay. The ATP levels of cells treated with complete growth medium in a humidified incubator were used as normoxic control. mBECs and hBECs incubated in OGD medium for 24 h were used as OGD control (**Fig. 5a-d**).

OGD exposure led to about a 70% reduction in mBEC ATP levels compared to normoxic mBECs (**Fig. 5 a-b**), whereas OGD reduced hBEC ATP levels to about 65% (**Fig. 5c-d**). OGD-mediated decreases in BEC ATP levels were statistically significant ($p<0.0001$) compared to untreated normoxic cells. Recipient OGD mBECs treated with mBEC- (**Fig. 5a**) and hBEC-MVs (**Fig. 5b**) at a dose as low as 1 μg per well showed a statistically significant ($p<0.05$) increase in cellular ATP levels compared to untreated OGD mBECs. Increasing the MV concentration showed a significant ($p<0.0001$) increase in BEC ATP levels (**Fig. 5a-b**). Notably, mBEC-MVs showed a greater increase in recipient mBEC ATP levels (**Fig. 5a**) compared to hBEC-MVs

(**Fig. 5b**) at all tested doses. In contrast, OGD mBECs treated with EXOs showed no significant increase in cellular ATP levels (**Fig. 5a-b**), likely due to the lower mitochondrial load in EXOs.

Moreover, recipient OGD hBECs treated with mBEC- (**Fig. 5c**) and hBEC-MVs (**Fig. 5d**) showed a concentration-dependent significant ($p<0.0001$) increase in cellular ATP levels compared to untreated OGD hBECs. OGD hBECs treated with EXOs showed a statistically significant ($p<0.0001$) increase in cellular ATP levels (**Fig. 5c-d**). It should be noted that MV-mediated increase in hBEC ATP levels was significantly ($p<0.0001$) greater than EXOs (**Fig. 5c-d**). Notably, mBEC-MVs increased cellular ATP levels to a greater magnitude than hBEC-MVs in recipient mBECs (**Fig. 5a-b**) and hBECs (**Fig. 5c-d**). In conclusion, mBEC-MVs outperformed hBEC-MVs in increasing ischemic BEC ATP levels.

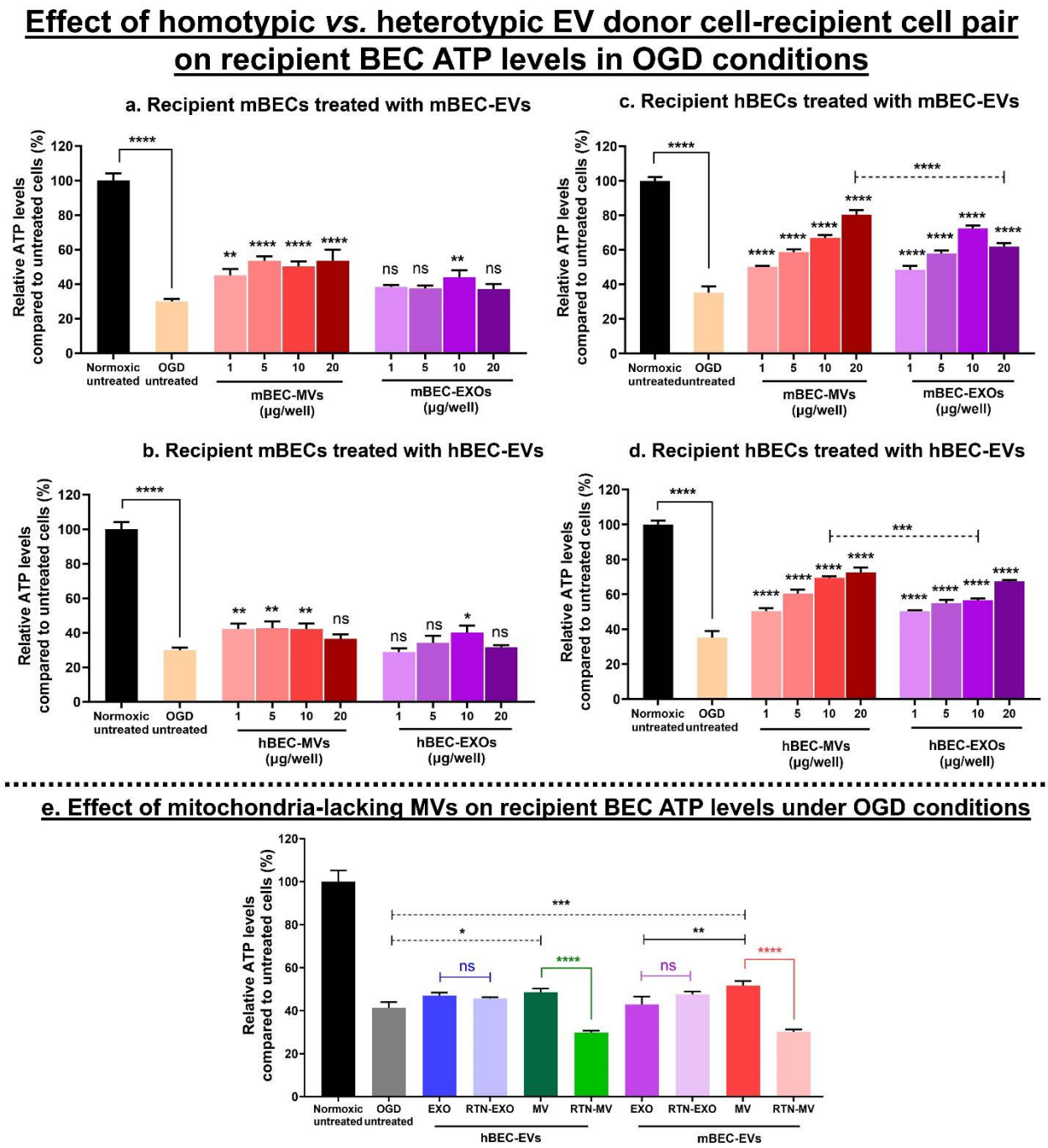

Figure 5: Effect of mBEC- and hBEC-EVs on recipient oxygen-glucose-deprived BEC ATP levels. mBECs and hBECs were cultured in 96-well plates in a humidified incubator at 37°C. Confluent monolayers were exposed to OGD medium in a hypoxic chamber for four hours. Post-OGD, the cells were treated with mBEC- and hBEC-EXOs and MVs at indicated amounts in OGD medium for 24 h. Cell treated with complete growth medium was used as normoxic control, whereas cells treated with only OGD medium was used as OGD control. Post-treatment, treatment mixtures were removed, and cells were incubated with a 1:1 mixture of fresh growth medium and Cell titer Glo reagent. The relative luminescence units (RLU) in each well were measured using a SYNERGY HTX multimode plate reader

at 1 s integration time. Relative ATP levels were calculated by normalizing the RLU of treatment groups to the RLU of normoxic untreated cells in complete growth medium. The effects of mBEC-derived EVs on recipient mBECs **(a)**, hBEC-derived EVs on recipient mBECs **(b)**, mBEC-derived EVs on recipient hBECs **(c)**, and hBEC-derived EVs on recipient hBEC ATP levels **(d)** were statistically evaluated compared to OGD control. **(e)** *Effect of mitochondria-lacking MVs on recipient BEC ATP levels.* OGD-exposed hBECs were treated with mBEC and hBEC-naïve EVs and RTN-EVs for 24 h in OGD conditions. RTN-EVs were isolated from donor BECs pre-exposed to 0.25 µM RTN. After incubation, the treatment mixture was removed, and the ATP assay was performed. Relative ATP levels were calculated by normalizing the RLU of treatment groups to the RLU of normoxic control. Data represents mean ± SD (n = 3). * $p < 0.05$, ** $p < 0.01$, *** $p < 0.001$, **** $p < 0.0001$, ns: non-significant.

Furthermore, to determine whether EV-mediated increases in recipient BEC ATP levels is a function of EV mitochondrial components, we studied the effect of EVs isolated from cells with impaired mitochondrial function. EVs with impaired mitochondrial function were isolated from the conditioned medium of hBECs or mBECs pretreated with 0.25 µM RTN. Recipient hBECs were treated with naïve EXOs, naïve MVs, RTN-EXOs, or RTN-MVs for 24 h under OGD conditions. OGD hBECs (**Fig. 5e**) showed a significant ($p<0.0001$) decrease in cellular ATP levels compared to normoxic BEC ATP levels. OGD hBECs treated with hBEC- and mBEC-EXOs did not show any increase in ATP levels compared to untreated OGD cells (**Fig. 5e**). OGD BECs treated with hBEC- and mBEC-MVs showed a significant ($p<0.01$) increase in OGD BEC ATP levels (**Fig. 5e**). There is no significant difference between BEC ATP levels treated with naïve EXOs *vs.* RTN-EXOs (**Fig. 5e**), suggesting that inhibition of donor hBEC mitochondrial function did not affect the ATP-increasing functionality of EXOs. Notably, RTN-MVs significantly reduced hBECs ATP levels compared to naïve MV-treated BECs (**Fig. 5e**), suggesting that inhibition of donor cell mitochondrial function reduces MV-mediated increase in BEC ATP levels. RTN-MVs mediated decrease in BEC ATP levels was consistent for MVs isolated from hBECs and mBECs (**Fig. 5e**). Overall, our results suggested that MV-mediated

increase in cellular ATP levels, regardless of EV donor species, is a function of MV mitochondria.

3.5. mBEC-MVs outperformed hBEC-MVs in increasing mitochondrial respiration of recipient OGD mBECs

The effect of mBEC- or hBEC-EV exposure on recipient mBEC mitochondrial function was evaluated using the Seahorse analysis (**Fig. 6**). OGD BECs were treated with different doses of EVs diluted in OGD medium for 24 h. The selected doses: 0.3, 3.3 and 13.2 µg EV protein are equivalent to ~3, 30 and 120 µg/cm^2 per well of the Seahorse plate (surface area per well: 0.11 cm^2). First, recipient mBECs exposed to OGD conditions significantly decreased OCR compared to untreated normoxic control (**Fig. 6**), suggesting that OGD significantly reduced cellular oxidative phosphorylation. OGD mBECs treated with mBEC- and hBEC-EXOs did not show any statistical increase in oxygen consumption rate (**OCR**) compared to untreated OGD control (**Fig. 6**). A low dose of MVs (0.3 µg/well) did not increase mitochondrial respiration of OGD mBECs (**Fig. 6**). mBECs treated with 3.3 and 13.3 µg/well mBEC- and hBEC-MVs showed a statistically significant (mBEC-MVs: $p<0.001$, hBEC-MVs: $p<0.05$) increases in OCR compared to untreated OGD control (**Fig. 6**). Notably, mBEC-MVs increased mBEC mitochondrial respiration to significantly ($p<0.001$) greater extent than hBEC-MVs (**Fig. 6**). Overall, hBEC- and mBEC-MVs significantly increased recipient mBEC and hBEC mitochondrial respiration compared to untreated and EXO-treated ischemic mBECs. Homotypic mBEC-MVs outperformed hBEC-MVs in increasing recipient mBECs mitochondrial respiration. Collectively, our data suggests that MVs derived from the same species as the recipient species, a.k.a.,

homotypic pairs (recipient mBECs treated with mBEC-MVs), show improved mitochondrial respiration than heterotypic pairs.

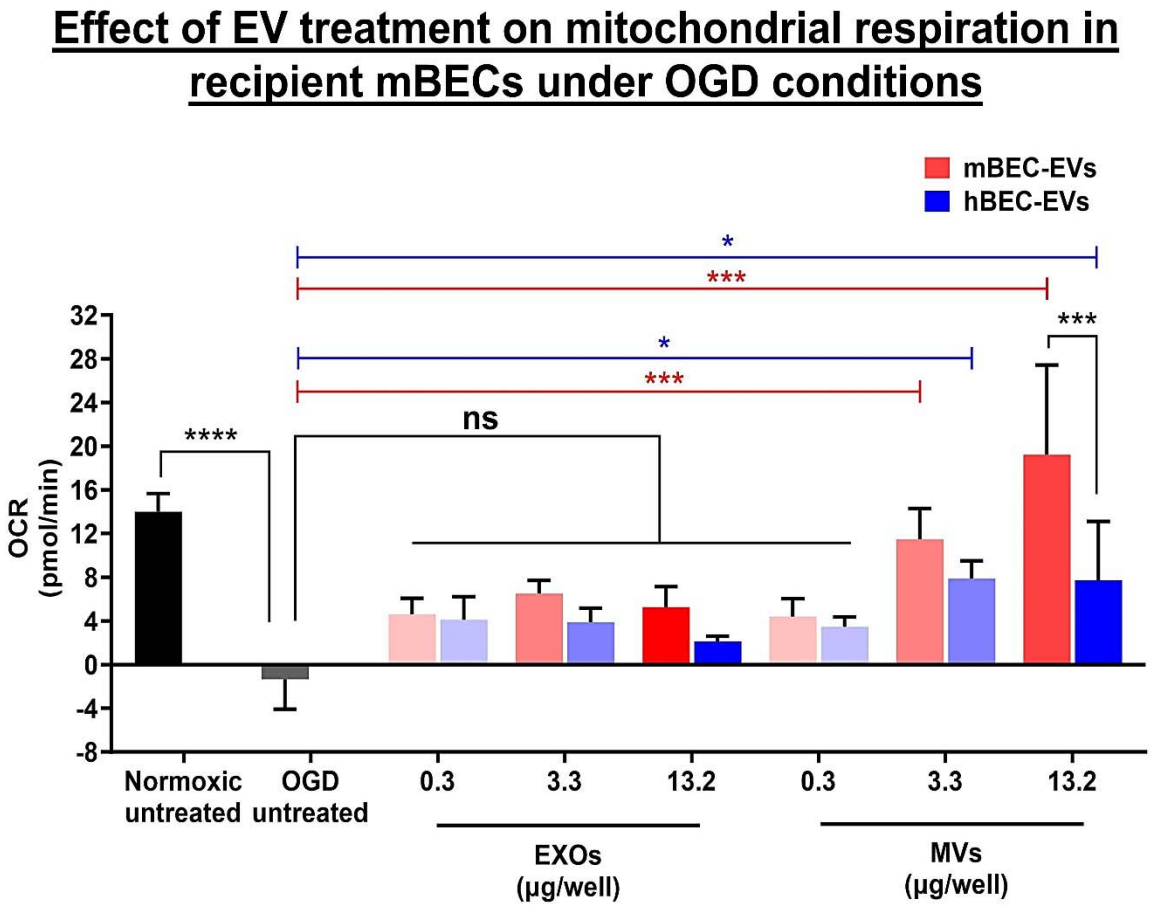

Figure 6: Effect of mouse and human BEC-derived EVs on recipient mBEC mitochondrial respiration under OGD conditions. mBECs were cultured in a Seahorse XF96 plate for four days at 20,000 cells/well. Confluent mBECs were incubated with OGD medium in a hypoxic chamber for four hours. Post-OGD exposure, cells were incubated with mBEC and hBEC-EVs at indicated doses diluted in OGD medium for 24 h. Post-treatment, the medium was replaced with DMEM. Maximum oxygen consumption rate (OCR) in mBEC was analyzed using the Seahorse XFe96 analyzer. Data represents mean±SD (n=3). * $p<0.05$, ** $p<0.01$, *** $p<0.001$, **** $p<0.0001$.

3.6. Intravenously injected mBEC-MVs demonstrate improved post-stroke outcomes in a mouse middle cerebral artery occlusion (MCAo) model of ischemic stroke

We evaluated the therapeutic efficacy of mBEC-MVs on resulting mouse brain infarct volumes and neurological functions in a mouse MCAo model of ischemic stroke. The mouse MCA was occluded using a silicon filament for 90 min to induce cerebral ischemia in mice, and reperfusion was initiated by withdrawing the filament. mBEC-derived MVs at 100 μg total MV protein in 200 μL of PBS were intravenously injected two hours after ischemic onset, and mice treated with PBS were used as vehicle control. Twenty-four hours post-treatment, mice were euthanized, and brain infarct volumes were analyzed using TTC-stained sections by a blinded investigator. The brain sections of mice treated with mBEC-EVs showed notably reduced infarct volume (white region) and showed greater viable tissue (red region) compared to the infarct volumes in mice treated with vehicle control (**Fig. 7a**). A quantitative analysis of the total hemispheric infarct volume showed that MV-treated mice brain sections showed about a 45% reduction ($p<0.01$) in infarct volume compared to PBS-treated mice (**Fig. 7b**). We also did not observe any difference in treatment-related mortalities, suggesting that mBEC-MVs are safe when administered intravenously to the mice.

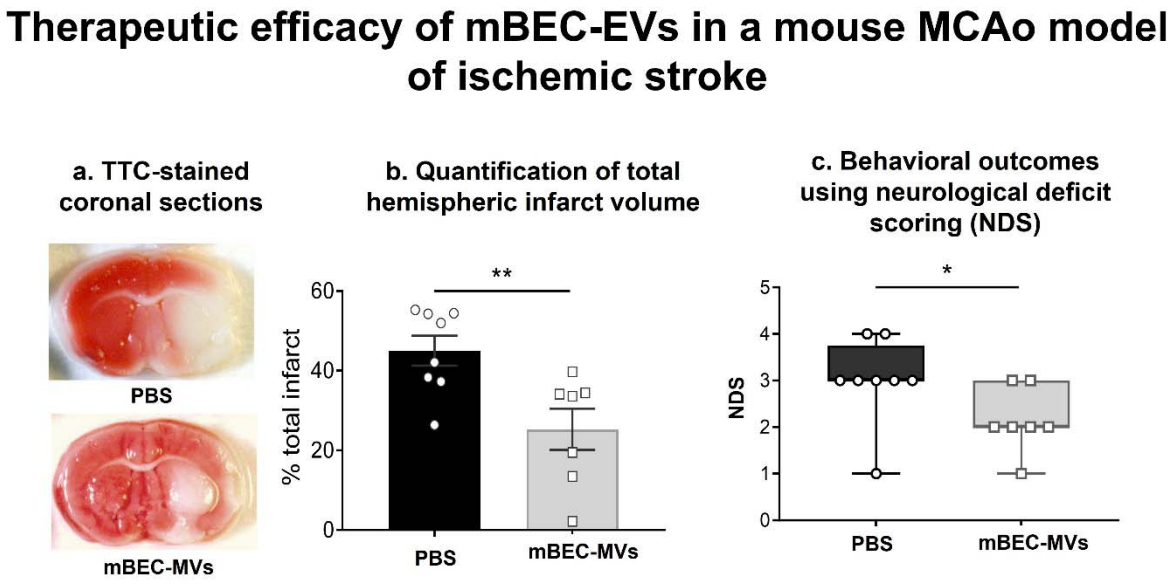

Figure 7: IV administration of mBEC-derived mitochondria-containing MVs showed neuroprotection in a mouse MCAo model of stroke. Young male C57BL/6 mice (8–12 weeks) were subjected to middle cerebral artery occlusion for 90 min to induce ischemic stroke. Reperfusion was initiated by withdrawing the filament. Two hours after ischemic onset, mice were treated with either mBEC-MVs (100 μg MV protein in 200 μL PBS) or vehicle control (200 μL of PBS). Twenty-four hours post-reperfusion, mice were euthanized and brains were analyzed for infarct size using TTC-stained sections. (a) representative TTC stained coronal section of PBS- or MV-treated MCAo mice. (b) Quantitative analysis of total hemispheric brain section infarct volume of MV (n=7) or PBS (n=8) treated mice. The data represents mean±SEM. The statistical difference between treatment and control group was performed using unpaired student's t-test. (c) Behavioral outcomes were measured using NDS at 24 hours post-treatment in MV- and PBS-treated MCAo mice. The statistical difference between treatment and control group was determined using the Mann-Whitney U test. *$p<0.05$, **$p<0.01$

We further studied the effects of MV administration on behavioral outcomes in the MCAo mice, again using a blinded investigator (**Fig. 7c**). Twenty-four hours post-treatment, mice were observed for their locomotor activities, and neurological deficit scores (**NDS**) of MV-treated mice were compared against vehicle controls. NDS scores of MV-treated mice were significantly ($p<0.05$) lower compared to vehicle controls, suggesting that IV-administration of mBEC-derived mitochondria-containing MVs significantly improved post-stroke behavioural outcomes of MCAo mice.

4. Discussion

This study investigated the effect of homotypic *vs.* heterotypic EV donor cell-recipient cell pair on MV mitochondria functionality in the recipient BECs. We evaluated the effect of mBEC-derived mitochondria-containing MVs on the metabolic function of recipient ischemic BECs and neuroprotective effects in a mouse MCAo model of stroke. Ischemic stroke-induced OGD leads to mitochondrial dysfunction in BECs, resulting in cell death and BBB breakdown. We rationalized that delivery of exogenous MV mitochondria into BECs can restore cellular metabolic functions and limit post-stroke neurological dysfunction [33].

EV donor cell type and species are factors that can significantly contribute to the therapeutic efficiencies of EVs [33, 34]. BECs contain about five-fold greater amounts of mitochondria than peripheral endothelial cells [8, 9]; and therefore, BEC-derived EVs potentially allow incorporation of a greater innate mitochondrial load than EVs from other cell types. BEC-EV membranes contain surface proteins such as transferrin receptor, insulin receptor, integrins, intercellular adhesion molecules, and CD46 [45-48], facilitating EV interactions with BBB surface receptors and subsequently allowing internalization into recipient BECs. Our previous study demonstrated that hBEC-MVs contain mitochondria [31, 36]. hBEC-MVs transferred mitochondria that colocalized with the mitochondrial network of the recipient BECs. As a consequence, hBEC-MVs increased ischemic hBEC ATP levels and mitochondrial respiration. A pilot study (n=4 mice) of *IV* injected hBEC-MVs in a mouse MCAo model of ischemic stroke showed a trend towards a potential efficacy signal [31]. We rationalized that a heterotypic combination of EV source species (hBEC-EVs) and recipient animal species (mouse model of stroke) likely contributed to the sub-optimal therapeutic efficacy of hBEC-MVs in the mouse

stroke model. Therefore, in this work, we hypothesized that IV administration of *m*BEC-MVs may show a superior reduction in brain infarct volume and improve neurological functions in MCAo mice.

In this work, we compared mBEC- *vs*. hBEC-MVs in terms of their (1) physicochemical properties and biomarkers and (2) capabilities to transfer the innate MV mitochondrial load into recipient mBECs or hBECs—we compared the levels of transfer between homotypic *vs*. heterotypic EV donor cell-recipient cell pairs. We further determined if ischemic conditions can affect MV mitochondria transfer into recipient OGD BECs. Finally, we evaluated the therapeutic efficacy of mBEC-MVs in a mouse MCAo model of ischemic stroke. Our results showed that irrespective of the donor cell species, both mBEC- and hBEC-MVs contained mitochondria, and EXOs lacked mitochondria. mBEC-EVs transferred their mitochondrial components into both recipient mBECs and hBECs. OGD conditions significantly reduced MV mitochondrial transfer compared to normoxic conditions. mBEC-MVs outperformed hBEC-MVs in increasing recipient ischemic mBEC ATP levels and oxygen consumption rate. Rotenone-mediated inhibition of donor BEC mitochondrial function significantly reduced MV mitochondria ATP-increasing functionality in recipient BECs, confirming that MV-mediated increases in recipient ischemic BEC ATP levels were a function of innate MV mitochondria. Lastly, *IV*-injected mBEC-MVs showed a statistically significant reduction in mouse brain infarct volume and significantly improved neurological functions in a mouse MCAo model of ischemic stroke.

We isolated EXOs and MVs from the conditioned medium of mBEC and hBECs using a differential ultracentrifugation method— a commonly used EV isolation method [49, 50]. EXOs showed characteristic particle diameters <200 nm, whereas the diameters of MVs were >200 nm (**Fig. 1a**), aligning with previous reports [17, 25, 32, 35, 51]. There were no significant differences in the particle diameters between mBEC- and hBEC-EXOs (**Fig. 1a**). In contrast, mBEC-MVs showed significantly higher particle diameters than hBEC-MVs (**Fig. 1a**). The net negative zeta potentials on EV membrane (**Fig. 1a**) are likely due to EV membrane phospholipid components such as phosphatidylinositol, phosphatidylserine, and glycosylated lipid derivatives [52, 53]. The natural process of EV biogenesis likely results in heterogenous EV sub-populations, manifesting as broad dispersity indices (**Fig. 1a**) that seemed consistent for human and mouse species-derived EVs. We observed similarities in the morphology of EXOs and MVs irrespective of EV donor species (mouse *vs*. human, **Fig. 1b**). EV characterization using western blotting (**Fig. 1c**) showed that EXOs and MVs have minimal endoplasmic reticulum contaminants, suggesting the purity of isolated EVs. CD63 and CD9, tetraspanin markers associated with exosomal cargo selection, binding, and uptake of EXOs by target cells [54], were expressed in EXOs derived from both species. ADP-ribosomal factor, **ARF6**, a GTP binding protein potential for cell migration/invasion, was selectively expressed MVs, consistent with a published report [55]. Moreover, EXOs and MVs contained cytosolic components such as GAPDH. Collectively, human and mouse BEC-derived EVs expressed characteristic protein biomarkers.

TEM analysis of cross-sectioned EVs showed that MV contained one or multiple mitochondria with heterogenous sizes and shapes in the MV lumen, whereas EXOs lack

electron-dense structures (**Fig. 2a**). The morphology of mitochondria-containing MVs were comparable between mBEC- and hBEC-EVs. Notably, the mitochondrial structures in MVs (**Fig. 2a**) were similar to the extracellular free mitochondria isolates and mitochondria in EV lumen reported in the published literature [17, 18, 48, 56]. Phinney *et al.* demonstrated the selective packaging of mitochondria in MVs while EXOs carried mtDNA, but not mitochondria [17]. The authors demonstrated that overexpression of Phosphatase and tensin homolog-induced kinase 1/Parkin proteins and suppression of Miro 1/2 protein on the outer mitochondrial membrane leads to mitochondria-cytoskeletal interactions [17]. The resulting complexes migrate towards the plasma membrane, package into cell buds, and pinching of these cell buds secretes mitochondria-containing MVs into extracellular spaces [17]. We further confirmed the presence of mitochondrial protein ATP5A, a subunit of the ATP synthase complex responsible for the synthesis or hydrolysis of ATP [57], in EXOs and MVs derived from mBECs and hBECs. A considerably greater expression of ATP5A in hBEC- and mBEC-MVs compared to EXOs (**Fig. 2b**), likely indicates a greater mitochondrial load in MVs than EXOs. Additionally, MVs selectively expressed mitochondrial structural protein TOMM20 (**Fig. 2b**), an outer mitochondrial membrane protein that regulates the import of specific proteins from the cytosol [58], confirming the presence of mitochondria in MVs but not in EXOs aligning with results of our TEM analysis (**Fig. 2a**). Overall, our results aligned with published reports [18, 30] demonstrating the presence of mitochondrial proteins in MVs. Ikeda *et al.* showed the presence of ATP5A proteins in human cardiomyocyte-derived mitochondria-containing MVs [18], whereas Silva *et al.* showed human mesenchymal stromal cell-derived MVs expressed TOMM20 [30]. Collectively, mBEC- and hBEC-MVs contained structural and functional mitochondrial

proteins, suggesting the consistency of MVs to package mitochondria irrespective of the donor cell species.

We further investigated the effects of (1) donor EV and recipient BEC species and (2) oxygen-glucose deprived *vs*. normoxic conditions on the extent of EV mitochondrial transfer. We labelled donor BEC mitochondria using MitoT-red, a mitochondrial membrane potential dye that stains polarized mitochondria [59, 60], and isolated EVs from the conditioned medium of mitochondria-prestained donor BECs. Our fluorescence microscopy results showed MV mitochondria signals in recipient BECs irrespective of the MV donor and recipient BEC species (**Fig. 3a-b**). Interestingly, mBEC-MVs showed a greater extent of mitochondria transfer into recipient normoxic BECs than mBEC-EXOs, hBEC-MVs and hBEC-EXOs at the highest tested dose (**Fig. 3c-d**). Noteworthy, mBEC-MVs showed substantially higher average MV particle diameters than hBEC-MVs (**Fig. 1a**). We speculate that mBECs produce large MVs with a greater mitochondrial load than hBEC counterparts. As a result, at the same total EV protein dose, mBEC-MVs showed greater mitochondrial transfer into recipient BECs than hBEC-MVs. Our results align with the *in vivo* study by Banks *et al*. [20] that investigated the effect of parent cell line species using EVs from cancerous *vs*. non-cancerous cells on EXO pharmacokinetics, brain distribution, and extent of BBB crossing in mice. The authors showed that all EXOs derived from mouse, human, cancerous, and non-cancerous donor cell lines crossed BBB, but their transport from blood to brain parenchyma varied from 58% to 92% compared to albumin control [20]. Importantly, mouse cell line-derived EXOs showed greater brain transport than human cell line-derived EXOs [20]. EXO membrane proteins, including CD46, ICAM1, and integrin, facilitate their transport to the BBB via adsorptive transcytosis [20].

Furthermore, we investigated the effect of OGD conditions on MV mitochondria transfer in recipient BECs using flow cytometry analysis. Alteplase-mediated dissolution of blood clots, the front-line treatment for stroke, restores blood flow (*i.e.*, reperfusion). Our goal is to deliver mitochondria-containing MVs during the reperfusion phase but OGD-mediated reduction in BEC metabolic functions may affect their EV uptake efficiency compared to healthy (normoxic) conditions. Therefore, we wanted to determine if OGD BECs can also internalize BEC-EVs. Recipient BECs were treated with MitoT-red-EVs at 10, 30, and 60 µg EV protein/well under normoxic and OGD conditions and %MitoT+ve cells were analyzed using flow cytometry. Our results demonstrated MitoT+ve cells in OGD BECs in all homotypic *vs*. heterotypic EV donor-recipient cell pairs (**Fig. 4 a-d**), indicating the potential of MVs to be internalized during ischemic conditions as well as normoxic conditions. Interestingly, recipient OGD BECs showed reduced MV mitochondrial signals compared to normoxic BECs irrespective of donor EV-recipient cell species (**Fig. 4a-d**). OGD conditions likely compromised cellular metabolic functions, translating to reduced EV internalization into recipient BECs. Hema *et al.* showed that prolonged hypoxic exposure decreased clathrin-independent endocytic uptake while clathrin-mediated endocytosis remained unaffected [61].

Mitochondrial oxidative phosphorylation produces 80-90% of cellular ATP, and OGD-induced mitochondrial dysfunction significantly reduces cellular ATP levels. First, mBECs and hBECs were incubated with OGD medium in a hypoxic chamber for four hours. Our data showed that four hours of OGD exposure reduces about 60% of BEC ATP levels compared to untreated normoxic BECs, which is consistent with the published reports [11, 62]. After OGD

exposure, mBECs and hBECs were treated with hBEC and mBEC-EVs for 24 h. Post-treatment, the relative ATP levels of BECs treated with EVs were compared to untreated OGD-exposed BECs. Our data showed that mBEC-MVs outperformed in increasing recipient OGD BEC ATP levels compared to mBEC-EXOs, hBEC-EXOs, and hBEC-MVs. Importantly, rotenone-mediated inhibition of donor BEC mitochondrial function significantly reduced ATP-increasing functions of MVs to a much greater extent than RTN-EXOs. This data suggested that an MV-mediated increase in recipient BEC ATP levels is a function of MV mitochondria, which is in agreement with our previous studies [31, 36]. As EXOs lack mitochondria, rotenone-mediated inhibition of donor mitochondria minimally affected EXO-mediated increases in ATP levels.

O'Brien *et al.* demonstrated that human mesenchymal stromal cell-derived MVs increased recipient human cardiomyocyte ATP levels [47]. The authors showed that MV transferred their mitochondria into recipient cells and colocalized with endogenous cell mitochondria. MV treatment increased cellular ATP levels and suppressed apoptosis in doxorubicin-injured cardiomyocytes [47]. Silva *et al.* showed that human pulmonary microvascular endothelial cells treated with human MSC-derived MVs showed a three-fold increase in recipient cellular ATP levels and a six-fold increase in mitochondrial respiration [30]. Rhodamine-mediated inhibition of MV mitochondrial functions did not increase endothelial ATP levels and mitochondrial respiration, suggesting that MV-mediated increase in recipient cell bioenergetics is a function of the innate MV mitochondrial load [30].

We further evaluated the homotypic *vs.* heterotypic EV donor-recipient cell effect on the EV-mediated modulation in recipient ischemic mBEC mitochondrial respiration using Seahorse

assays. The Seahorse extracellular flux analyzer facilitates real-time measurements of the oxygen consumption rate, an indicator of mitochondrial respiration, and extracellular acidification rate, an indicator of glycolytic capacity in live intact cells [63, 64]. Our data showed that mBEC exposed to OGD substantially reduced cellular mitochondrial respiration compared to untreated normoxic BECs (**Fig. 6**). We observed that irrespective of the EV donor BEC species, EXOs did not increase OGD BEC mitochondrial respiration (**Fig. 6)**. Both mBEC- and hBEC-MVs showed a dose-dependent increase in recipient OGD mBEC mitochondrial respiration (**Fig. 6**). mBEC-MVs increased cellular oxidative phosphorylation compared to hBEC-MVs in the recipient mBECs (**Fig. 6**). Our data align with the published reports [17, 18, 30, 32] on EV-mediated increase in recipient cellular mitochondrial respiration. For instance, Ikeda *et al.* showed human cardiomyocyte-derived mitochondria-rich MVs treated with hypoxic human cardiomyocytes showed a significant increase in basal, ATP-induced, and maximum mitochondrial respiration compared to untreated hypoxic cells [18]. Our results indicate that homotypic donor EV-recipient cell pairs outperform heterotypic donor EV-recipient cells in increasing recipient BEC mitochondrial functions.

Collectively, our data thus far showed that mBEC-MVs outperformed hBEC-MVs in MV mitochondrial transfer (**Fig. 3 and 4**), increasing ischemic BEC ATP levels (**Fig. 5**), and mitochondrial respiration (**Fig. 6**). Based on the superior performance of mBEC-MVs, we *IV*-administered mBEC-MVs after ischemia/reperfusion injury in a mouse MCAo model of ischemic stroke. Our data revealed a statistically significant reduction in brain infarct volume compared to vehicle-treated mice (**Fig. 7a-b**). Importantly, mBEC-MVs were administered two hours after reperfusion, simulating a clinical scenario of delayed administration, and yet, we

noted a 45% reduction in infarct volume to vehicle-injected mice. Importantly, mice treated with mBEC-MVs showed a statistically significant improvement (p=<0.5) in behavioral outcomes post-ischemia/reperfusion injury (**Fig. 7c**). It should be noted that this is the first demonstration of mBEC-MV-mediated cerebroprotection and improved behavioral outcomes in a mouse model of ischemic stroke.

It should be noted that we used young male mice for MCAo studies as the model has been standardized, allows to exclude estrogen-related neuroprotection effects, and the mortality rates are much lower in younger mice compared to aged mice. MV administration did not show any treatment-related mortalities and showed significantly improved neurological functions 24 h post-stroke onset. However, we acknowledge that the mice were analyzed post a short end-point, and therefore, we intend to measure chronic post-stroke recovery (72 h post-administration of treatment or later) and in aged mice in future studies. In addition, our future studies will (1) evaluate the effects of different MV doses, (2) determine whole blood and brain pharmacokinetics and systemic biodistribution of MV mitochondria in healthy and MCAo mice, and (3) determine therapeutic efficacy of MV mitochondria in aged male and female mice. The cell assays we have reported here in were not designed to detect any potential sex differences in EV mitochondrial load. Pulmonary ECs from male mice showed an increased basal and maximal respiration rates, and were more sensitive to pharmacologically-impaired mitochondrial function compared to cells from female mice [65]. If our future experiments reveal sex differences, we will compare primary BECs [66] isolated from male *vs*. female mice in our subsequent studies.

5. Conclusions

Our results suggest that mBEC-MVs likely contain greater mitochondrial load than hBEC-MVs. Homotypic donor EV-recipient cell pairs outperform heterotypic donor EV-recipient cells in increasing recipient BEC ATP levels and mitochondrial respiration. *IV* administration of mBEC-MVs decreased brain infarct volume and improved behavioral outcomes compared to vehicle-treated controls in a mouse model of ischemic stroke. Our data demonstrates that mBEC-derived mitochondria-containing MVs is a potent approach to improve post-stroke outcomes.

6. Author contributions

Conceptualization, Formal analysis, Methodology, Funding acquisition, Project administration, Resources, Supervision D.S.M Investigation, Data curation, Formal analysis, Methodology K.M.D, V.R.V, D.B.S., S.S.S, L.D.M and D.S.M Transmission electron microscopy K.M.D and D.B.S *In vitro* assays K.M.D, E.E.H, D.G *In vivo* experiments V.R.V, V.A.Q, M.E.M Seahorse studies K.M.D, K.S.R, D.S.M. Physicochemical characterization K.M.D, E.E.H, D.G, M.C, J.M, S.Z Flow cytometry K.M.D, D.S.M Fluorescence microscopy K.M.D, D.S.M Data analysis K.M.D, D.S.M Manuscript writing K.M.D., V.V., L.D.M., D.S.M.

7. Acknowledgements

This work was supported via start-up funds for the Manickam laboratory from Duquesne University (DU) to the PI. We would like to acknowledge the Neurodegenerative Undergraduate Research Experience for funding EEH through a grant from the National Institute of Neurological Disorders and Stroke (R25NS100118). The authors are thankful to Dr. Rehana K. Leak (DU) for the Olympus epifluorescence microscope and Odyssey imager support. The authors are grateful to Drs. Lauren O'Donnell, Manisha Chandwani, and Yashika Kamte (DU) for flow cytometry support.

Data availability. The raw/processed data required to reproduce these findings can be obtained from the corresponding author upon request.

Declaration of interests. The authors declare that they have no known competing financial interests or personal relationships that could have appeared to influence the work reported in this paper.

8. References

1. Liu F, Lu J, Manaenko A, Tang J, Hu Q. Mitochondria in Ischemic Stroke: New Insight and Implications. Aging Dis. 2018;9(5):924-37.
2. Yang J-L, Mukda S, Chen S-D. Diverse roles of mitochondria in ischemic stroke. Redox biology. 2018;16:263-75.
3. Kluge MA, Fetterman JL, Vita JA. Mitochondria and endothelial function. Circulation research. 2013;112(8):1171-88.
4. Bustamante-Barrientos FA, Luque-Campos N, Araya MJ, Lara-Barba E, de Solminihac J, Pradenas C, Molina L, Herrera-Luna Y, Utreras-Mendoza Y, Elizondo-Vega R, Vega-Letter AM, Luz-Crawford P. Mitochondrial dysfunction in neurodegenerative disorders: Potential therapeutic application of mitochondrial transfer to central nervous system-residing cells. Journal of Translational Medicine. 2023;21(1):613.
5. Benjamin EJ, Blaha MJ, Chiuve SE, Cushman M, Das SR, Deo R, de Ferranti SD, Floyd J, Fornage M, Gillespie C, Isasi CR, Jiménez MC, Jordan LC, Judd SE, Lackland D, Lichtman JH, Lisabeth L, Liu S, Longenecker CT, Mackey RH, Matsushita K, Mozaffarian D, Mussolino ME, Nasir K, Neumar RW, Palaniappan L, Pandey DK, Thiagarajan RR, Reeves MJ, Ritchey M, Rodriguez CJ, Roth GA, Rosamond WD, Sasson C, Towfighi A, Tsao CW,

Turner MB, Virani SS, Voeks JH, Willey JZ, Wilkins JT, Wu JH, Alger HM, Wong SS, Muntner P. Heart Disease and Stroke Statistics-2017 Update: A Report From the American Heart Association. Circulation. 2017;135(10):e146-e603.
6. Abdullahi W, Tripathi D, Ronaldson PT. Blood-brain barrier dysfunction in ischemic stroke: targeting tight junctions and transporters for vascular protection. Am J Physiol Cell Physiol. 2018;315(3):C343-C56.
7. Nian K, Harding IC, Herman IM, Ebong EE. Blood-Brain Barrier Damage in Ischemic Stroke and Its Regulation by Endothelial Mechanotransduction. Frontiers in Physiology. 2020;11(1681).
8. Oldendorf WH, Cornford ME, Brown WJ. The large apparent work capability of the blood-brain barrier: A study of the mitochondrial content of capillary endothelial cells in brain and other tissues of the rat. Annals of Neurology. 1977;1(5):409-17.
9. Lee MJ, Jang Y, Han J, Kim SJ, Ju X, Lee YL, Cui J, Zhu J, Ryu MJ, Choi SY, Chung W, Heo C, Yi HS, Kim HJ, Huh YH, Chung SK, Shong M, Kweon GR, Heo JY. Endothelial-specific Crif1 deletion induces BBB maturation and disruption via the alteration of actin dynamics by impaired mitochondrial respiration. J Cereb Blood Flow Metab. 2020;40(7):1546-61.
10. Bernardo-Castro S, Sousa JA, Brás A, Cecília C, Rodrigues B, Almendra L, Machado C, Santo G, Silva F, Ferreira L, Santana I, Sargento-Freitas J. Pathophysiology of Blood–Brain Barrier Permeability Throughout the Different Stages of Ischemic Stroke and Its Implication on Hemorrhagic Transformation and Recovery. Frontiers in Neurology. 2020;11(1605).
11. Park H-H, Han M-H, Choi H, Lee YJ, Kim JM, Cheong JH, Ryu JI, Lee K-Y, Koh S-H. Mitochondria damaged by Oxygen Glucose Deprivation can be Restored through Activation of the PI3K/Akt Pathway and Inhibition of Calcium Influx by Amlodipine Camsylate. Scientific Reports. 2019;9(1):15717.
12. Tyagi N, Ovechkin AV, Lominadze D, Moshal KS, Tyagi SC. Mitochondrial mechanism of microvascular endothelial cells apoptosis in hyperhomocysteinemia. J Cell Biochem. 2006;98(5):1150-62.
13. Twig G, Elorza A, Molina AJA, Mohamed H, Wikstrom JD, Walzer G, Stiles L, Haigh SE, Katz S, Las G, Alroy J, Wu M, Py BF, Yuan J, Deeney JT, Corkey BE, Shirihai OS. Fission and selective fusion govern mitochondrial segregation and elimination by autophagy. EMBO J. 2008;27(2):433-46.
14. Todkar K, Chikhi L, Desjardins V, El-Mortada F, Pépin G, Germain M. Selective packaging of mitochondrial proteins into extracellular vesicles prevents the release of mitochondrial DAMPs. Nature Communications. 2021;12(1):1971.
15. Guescini M, Genedani S, Stocchi V, Agnati LF. Astrocytes and Glioblastoma cells release exosomes carrying mtDNA. J Neural Transm (Vienna). 2010;117(1):1-4.
16. Puhm F, Afonyushkin T, Resch U, Obermayer G, Rohde M, Penz T, Schuster M, Wagner G, Rendeiro AF, Melki I, Kaun C, Wojta J, Bock C, Jilma B, Mackman N, Boilard E, Binder CJ. Mitochondria Are a Subset of Extracellular Vesicles Released by Activated Monocytes and Induce Type I IFN and TNF Responses in Endothelial Cells. Circulation Research. 2019;125(1):43-52.
17. Phinney DG, Di Giuseppe M, Njah J, Sala E, Shiva S, St Croix CM, Stolz DB, Watkins SC, Di YP, Leikauf GD, Kolls J, Riches DW, Deiuliis G, Kaminski N, Boregowda SV, McKenna DH, Ortiz LA. Mesenchymal stem cells use extracellular vesicles to outsource mitophagy and shuttle microRNAs. Nat Commun. 2015;6:8472.
18. Ikeda G, Santoso MR, Tada Y, Li AM, Vaskova E, Jung J-H, O'Brien C, Egan E, Ye J, Yang PC. Mitochondria-Rich Extracellular Vesicles From Autologous Stem Cell–Derived Cardiomyocytes Restore Energetics of Ischemic Myocardium. Journal of the American College of Cardiology. 2021;77(8):1073-88.
19. Jean-Toussaint R, Lin Z, Tian Y, Gupta R, Pande R, Luo X, Hu H, Sacan A, Ajit SK. Therapeutic and prophylactic effects of macrophage-derived small extracellular vesicles in the attenuation of inflammatory pain. Brain Behav Immun. 2021;94:210-24.
20. Banks WA, Sharma P, Bullock KM, Hansen KM, Ludwig N, Whiteside TL. Transport of Extracellular Vesicles across the Blood-Brain Barrier: Brain Pharmacokinetics and Effects of Inflammation. Int J Mol Sci. 2020;21(12).
21. Murphy DE, de Jong OG, Brouwer M, Wood MJ, Lavieu G, Schiffelers RM, Vader P. Extracellular vesicle-based therapeutics: natural versus engineered targeting and trafficking. Experimental & Molecular Medicine. 2019;51(3):1-12.
22. Kodali M, Madhu LN, Reger RL, Milutinovic B, Upadhya R, Gonzalez JJ, Attaluri S, Shuai B, Gitai DLG, Rao S, Choi JM, Jung SY, Shetty AK. Intranasally administered human MSC-derived extracellular vesicles inhibit NLRP3-p38/MAPK signaling after TBI and prevent chronic brain dysfunction. Brain Behav Immun. 2023;108:118-34.
23. Drommelschmidt K, Serdar M, Bendix I, Herz J, Bertling F, Prager S, Keller M, Ludwig A-K, Duhan V, Radtke S, de Miroschedji K, Horn PA, van de Looij Y, Giebel B, Felderhoff-Müser U. Mesenchymal stem cell-

derived extracellular vesicles ameliorate inflammation-induced preterm brain injury. Brain Behav Immun. 2017;60:220-32.
24. Haraszti RA, Didiot M-C, Sapp E, Leszyk J, Shaffer SA, Rockwell HE, Gao F, Narain NR, DiFiglia M, Kiebish MA, Aronin N, Khvorova A. High-resolution proteomic and lipidomic analysis of exosomes and microvesicles from different cell sources. Journal of extracellular vesicles. 2016;5:32570-.
25. Dozio V, Sanchez J-C. Characterisation of extracellular vesicle-subsets derived from brain endothelial cells and analysis of their protein cargo modulation after TNF exposure. Journal of Extracellular Vesicles. 2017;6(1):1302705.
26. Tricarico C, Clancy J, D'Souza-Schorey C. Biology and biogenesis of shed microvesicles. Small GTPases. 2017;8(4):220-32.
27. Islam MN, Das SR, Emin MT, Wei M, Sun L, Westphalen K, Rowlands DJ, Quadri SK, Bhattacharya S, Bhattacharya J. Mitochondrial transfer from bone-marrow–derived stromal cells to pulmonary alveoli protects against acute lung injury. Nature Medicine. 2012;18(5):759-65.
28. Hough KP, Trevor JL, Strenkowski JG, Wang Y, Chacko BK, Tousif S, Chanda D, Steele C, Antony VB, Dokland T, Ouyang X, Zhang J, Duncan SR, Thannickal VJ, Darley-Usmar VM, Deshane JS. Exosomal transfer of mitochondria from airway myeloid-derived regulatory cells to T cells. Redox Biol. 2018;18:54-64.
29. Liu D, Dong Z, Wang J, Tao Y, Sun X, Yao X. The existence and function of mitochondrial component in extracellular vesicles. Mitochondrion. 2020;54:122-7.
30. Dutra Silva J, Su Y, Calfee CS, Delucchi KL, Weiss D, McAuley DF, O'Kane C, Krasnodembskaya AD. Mesenchymal stromal cell extracellular vesicles rescue mitochondrial dysfunction and improve barrier integrity in clinically relevant models of ARDS. European Respiratory Journal. 2021;58(1):2002978.
31. Dave KM, Stolz DB, Venna VR, Quaicoe VA, Maniskas ME, Reynolds MJ, Babidhan R, Dobbins DX, Farinelli MN, Sullivan A, Bhatia TN, Yankello H, Reddy R, Bae Y, Leak RK, Shiva SS, McCullough LD, Manickam DS. Mitochondria-containing extracellular vesicles (EV) reduce mouse brain infarct sizes and EV/HSP27 protect ischemic brain endothelial cultures. J Control Release. 2023;354:368-93.
32. D'Souza A, Burch A, Dave KM, Sreeram A, Reynolds MJ, Dobbins DX, Kamte YS, Zhao W, Sabatelle C, Joy GM, Soman V, Chandran UR, Shiva SS, Quillinan N, Herson PS, Manickam DS. Microvesicles transfer mitochondria and increase mitochondrial function in brain endothelial cells. J Control Release. 2021;338:505-26.
33. Dave KM, Stolz DB, Manickam DS. Delivery of mitochondria-containing extracellular vesicles to the BBB for ischemic stroke therapy. Expert Opinion on Drug Delivery.1-20.
34. Zhu X, Badawi M, Pomeroy S, Sutaria DS, Xie Z, Baek A, Jiang J, Elgamal OA, Mo X, Perle K, Chalmers J, Schmittgen TD, Phelps MA. Comprehensive toxicity and immunogenicity studies reveal minimal effects in mice following sustained dosing of extracellular vesicles derived from HEK293T cells. J Extracell Vesicles. 2017;6(1):1324730.
35. Dave KM, Zhao W, Hoover C, D’Souza A, S Manickam D. Extracellular Vesicles Derived from a Human Brain Endothelial Cell Line Increase Cellular ATP Levels. AAPS PharmSciTech. 2021;22(1):18.
36. Dave KM, Dobbins DX, Farinelli MN, Sullivan A, Milosevic J, Stolz DB, Kim J, Zheng S, Manickam DS. Engineering Extracellular Vesicles to Modulate Their Innate Mitochondrial Load. Cell Mol Bioeng. 2022;15(5):367-89.
37. Dai X, Chen J, Xu F, Zhao J, Cai W, Sun Z, Hitchens TK, Foley LM, Leak RK, Chen J, Hu X. TGFα preserves oligodendrocyte lineage cells and improves white matter integrity after cerebral ischemia. Journal of Cerebral Blood Flow & Metabolism. 2020;40(3):639-55.
38. Cardenes N, Corey C, Geary L, Jain S, Zharikov S, Barge S, Novelli EM, Shiva S. Platelet bioenergetic screen in sickle cell patients reveals mitochondrial complex V inhibition, which contributes to platelet activation. Blood. 2014;123(18):2864-72.
39. McCullough LD, Roy-O’Reilly M, Lai Y-J, Patrizz A, Xu Y, Lee J, Holmes A, Kraushaar DC, Chauhan A, Sansing LH, Stonestreet BS, Zhu L, Kofler J, Lim Y-P, Venna VR. Exogenous inter-α inhibitor proteins prevent cell death and improve ischemic stroke outcomes in mice. The Journal of Clinical Investigation. 2021;131(17).
40. Liu F, Yuan R, Benashski SE, McCullough LD. Changes in Experimental Stroke Outcome across the Life Span. Journal of Cerebral Blood Flow & Metabolism. 2009;29(4):792-802.
41. Venna VR, Weston G, Benashski SE, Tarabishy S, Liu F, Li J, Conti LH, McCullough LD. NF-κB contributes to the detrimental effects of social isolation after experimental stroke. Acta Neuropathol. 2012;124(3):425-38.
42. McCullough LD, Zeng Z, Li H, Landree LE, McFadden J, Ronnett GV. Pharmacological inhibition of AMP-activated protein kinase provides neuroprotection in stroke. J Biol Chem. 2005;280(21):20493-502.

43. Ritzel RM, Patel AR, Spychala M, Verma R, Crapser J, Koellhoffer EC, Schrecengost A, Jellison ER, Zhu L, Venna VR, McCullough LD. Multiparity improves outcomes after cerebral ischemia in female mice despite features of increased metabovascular risk. Proc Natl Acad Sci U S A. 2017;114(28):E5673-e82.
44. Ritzel RM, Pan SJ, Verma R, Wizeman J, Crapser J, Patel AR, Lieberman R, Mohan R, McCullough LD. Early retinal inflammatory biomarkers in the middle cerebral artery occlusion model of ischemic stroke. Mol Vis. 2016;22:575-88.
45. Venna VR, Benashski SE, Chauhan A, McCullough LD. Inhibition of glycogen synthase kinase-3β enhances cognitive recovery after stroke: the role of TAK1. Learn Mem. 2015;22(7):336-43.
46. Pospichalova V, Svoboda J, Dave Z, Kotrbova A, Kaiser K, Klemova D, Ilkovics L, Hampl A, Crha I, Jandakova E, Minar L, Weinberger V, Bryja V. Simplified protocol for flow cytometry analysis of fluorescently labeled exosomes and microvesicles using dedicated flow cytometer. J Extracell Vesicles. 2015;4:25530.
47. O'Brien CG, Ozen MO, Ikeda G, Vaskova E, Jung JH, Bayardo N, Santoso MR, Shi L, Wahlquist C, Jiang Z, Jung Y, Zeng Y, Egan E, Sinclair R, Gee A, Witteles R, Mercola M, Svensson KJ, Demirci U, Yang PC. Mitochondria-Rich Extracellular Vesicles Rescue Patient-Specific Cardiomyocytes From Doxorubicin Injury: Insights Into the SENECA Trial. JACC CardioOncol. 2021;3(3):428-40.
48. Hayakawa K, Esposito E, Wang X, Terasaki Y, Liu Y, Xing C, Ji X, Lo EH. Transfer of mitochondria from astrocytes to neurons after stroke. Nature. 2016;535(7613):551-5.
49. Yang D, Zhang W, Zhang H, Zhang F, Chen L, Ma L, Larcher LM, Chen S, Liu N, Zhao Q, Tran PHL, Chen C, Veedu RN, Wang T. Progress, opportunity, and perspective on exosome isolation - efforts for efficient exosome-based theranostics. Theranostics. 2020;10(8):3684-707.
50. Livshits MA, Khomyakova E, Evtushenko EG, Lazarev VN, Kulemin NA, Semina SE, Generozov EV, Govorun VM. Isolation of exosomes by differential centrifugation: Theoretical analysis of a commonly used protocol. Scientific Reports. 2015;5(1):17319.
51. Kanada M, Bachmann MH, Hardy JW, Frimannson DO, Bronsart L, Wang A, Sylvester MD, Schmidt TL, Kaspar RL, Butte MJ, Matin AC, Contag CH. Differential fates of biomolecules delivered to target cells via extracellular vesicles. Proceedings of the National Academy of Sciences. 2015;112(12):E1433-E42.
52. Konoshenko MY, Lekchnov EA, Vlassov AV, Laktionov PP. Isolation of Extracellular Vesicles: General Methodologies and Latest Trends. Biomed Res Int. 2018;2018:8545347.
53. El Andaloussi S, Mäger I, Breakefield XO, Wood MJA. Extracellular vesicles: biology and emerging therapeutic opportunities. Nature Reviews Drug Discovery. 2013;12(5):347-57.
54. Andreu Z, Yáñez-Mó M. Tetraspanins in extracellular vesicle formation and function. Front Immunol. 2014;5:442.
55. Muralidharan-Chari V, Clancy J, Plou C, Romao M, Chavrier P, Raposo G, D'Souza-Schorey C. ARF6-regulated shedding of tumor cell-derived plasma membrane microvesicles. Curr Biol. 2009;19(22):1875-85.
56. Hayakawa K, Chan SJ, Mandeville ET, Park JH, Bruzzese M, Montaner J, Arai K, Rosell A, Lo EH. Protective Effects of Endothelial Progenitor Cell-Derived Extracellular Mitochondria in Brain Endothelium. Stem Cells. 2018;36(9):1404-10.
57. Goldberg J, Currais A, Prior M, Fischer W, Chiruta C, Ratliff E, Daugherty D, Dargusch R, Finley K, Esparza-Moltó PB, Cuezva JM, Maher P, Petrascheck M, Schubert D. The mitochondrial ATP synthase is a shared drug target for aging and dementia. Aging Cell. 2018;17(2).
58. Yamamoto H, Itoh N, Kawano S, Yatsukawa Y-i, Momose T, Makio T, Matsunaga M, Yokota M, Esaki M, Shodai T, Kohda D, Hobbs AEA, Jensen RE, Endo T. Dual role of the receptor Tom20 in specificity and efficiency of protein import into mitochondria. Proceedings of the National Academy of Sciences of the United States of America. 2011;108(1):91-6.
59. Xiao B, Deng X, Zhou W, Tan EK. Flow Cytometry-Based Assessment of Mitophagy Using MitoTracker. Front Cell Neurosci. 2016;10(76):76.
60. Chazotte B. Labeling mitochondria with MitoTracker dyes. Cold Spring Harb Protoc. 2011;2011(8):990-2.
61. A. Naveena H, Bhatia D. Hypoxia Modulates Cellular Endocytic Pathways and Organelles with Enhanced Cell Migration and 3D Cell Invasion**. ChemBioChem.n/a(n/a):e202300506.
62. Liao L-X, Zhao M-B, Dong X, Jiang Y, Zeng K-W, Tu P-F. TDB protects vascular endothelial cells against oxygen-glucose deprivation/reperfusion-induced injury by targeting miR-34a to increase Bcl-2 expression. Scientific Reports. 2016;6(1):37959.
63. Smolina N, Bruton J, Kostareva A, Sejersen T. Assaying Mitochondrial Respiration as an Indicator of Cellular Metabolism and Fitness. Methods Mol Biol. 2017;1601:79-87.

64. Rose S, Frye RE, Slattery J, Wynne R, Tippett M, Pavliv O, Melnyk S, James SJ. Oxidative stress induces mitochondrial dysfunction in a subset of autism lymphoblastoid cell lines in a well-matched case control cohort. PLoS One. 2014;9(1):e85436.
65. Zemskova M, Kurdyukov S, James J, McClain N, Rafikov R, Rafikova O. Sex-specific stress response and HMGB1 release in pulmonary endothelial cells. PLoS One. 2020;15(4):e0231267.
66. Conchinha NV, Sokol L, Teuwen L-A, Veys K, Dumas SJ, Meta E, García-Caballero M, Geldhof V, Chen R, Treps L, Borri M, de Zeeuw P, Falkenberg KD, Dubois C, Parys M, de Rooij LPMH, Rohlenova K, Goveia J, Schoonjans L, Dewerchin M, Eelen G, Li X, Kalucka J, Carmeliet P. Protocols for endothelial cell isolation from mouse tissues: brain, choroid, lung, and muscle. STAR Protocols. 2021;2(3):100508.